SYNTHESIS OF HYDROXYAPATITE NANOPARTICLES FOR POLYNUCLEOTIDES DELIVERY I
N DENTISTRY

Miss Natthaya Thepphanao

A Thesis Submitted in Partial Fulfillment of the Requirements

for the Degree of Master of Science in Chemistry

Department of Chemistry

Faculty of Science

Chulalongkorn University

Academic Year 2018

การสังเคราะห์อนุภาคไฮดรอกซีแอพาไทต์ระดับนาโนเมตรสำหรับการนำส่งพอลินิวคลีโอไทด์ทางทันตกรรม

น.ส.ณัฐธยาน์ เทพเนาว์

วิทยานิพนธ์นี้เป็นส่วนหนึ่งของการศึกษาตามหลักสูตรปริญญาวิทยาศาสตรมหาบัณฑิต
สาขาวิชาเคมี ภาควิชาเคมี
คณะวิทยาศาสตร์ จุฬาลงกรณ์มหาวิทยาลัย
ปีการศึกษา 2561
ลิขสิทธิ์ของจุฬาลงกรณ์มหาวิทยาลัย

Thesis Title	SYNTHESIS OF HYDROXYAPATITE NANOPARTICLES FOR P OLYNUCLEOTIDES DELIVERY IN DENTISTRY
By	Miss Natthaya Thepphanao
Field of Study	Chemistry
Thesis Advisor	Numpon Insin

Accepted by the Faculty of Science, Chulalongkorn University in Partial Fulfillment of the Requirement for the Master of Science

.... Dean of the Faculty of Science

(Associate Professor Polkit Sangvanich)

THESIS COMMITTEE

.... Chairman

(Associate Professor Vudhichai Parasuk)

.... Thesis Advisor

(Numpon Insin)

.... Examiner

(Wipark Anutrasakda)

.... External Examiner

(Nisanart Charoenlap)

ระบบการนำส่งไมโครอาร์เอ็นเอด้วยอนุภาคไฮดรอกซีแอพาไทต์ระดับนาโนเมตรนับเป็นวิธีการรักษาหนึ่งที่สำคัญในการเหนี่ยวนำการสร้างกระดูกใหม่ ดังนั้น จึงเป็นที่น่าสนใจที่จะพัฒนาอนุภาคไฮดรอกซีแอพาไทต์เพื่อให้ได้ประสิทธิภาพการรักษาอย่างสูงสุด การศึกษานี้จัดทำขึ้นเพื่ออธิบายถึงอิทธิพลของลักษณะของอนุภาคไฮดรอกซีแอพาไทต์ต่อผลทางชีวภาพต่อเซลล์กระดูก โดยทำการสังเคราะห์อนุภาคที่มีขนาดแตกต่างกัน ได้อนุภาคที่มีรูปร่างแท่งขนาด 150-200 และ 100 นาโนเมตร และอนุภาคที่มีรูปร่างแตกต่างกัน ได้อนุภาครูปร่างแท่งยาวขนาด 100-150 นาโนเมตร จากนั้น จึงทำการเปรียบเทียบความเป็นพิษต่อเซลล์ ประสิทธิภาพในการเข้าสู่เซลล์ และความสามารถในการจับกับไมโครอาร์เอ็นเอ ผลการทดลองพบว่า อนุภาคที่มีรูปร่างแท่งและแท่งยาวขนาด 100-150 นาโนเมตรมีความเป็นพิษต่อเซลล์ต่ำและยังมีประสิทธิภาพในการเข้าสู่เซลล์สูงที่สุดอีกด้วย แต่อย่างไรก็ตาม อนุภาคทั้งสองกลับมีความสามารถในการจับกับไมโครอาร์เอ็นเอต่ำเนื่องจากมีพื้นผิวเป็นลบ ดังนั้น โมเลกุลประจุบวกคือ APTES และ PDMAEMA จึงถูกนำมาเชื่อมต่อบนผิวของอนุภาคที่มีรูปร่างแท่งยาวเพื่อตรวจสอบผลกระทบของประจุบนผิวต่อสมบัติทางชีวภาพของอนุภาค โดยพบว่าอนุภาคไฮดรอกซีแอพาไทต์ที่มี APTES บนผิวมีความเป็นพิษต่ำและมีประสิทธิภาพในการเข้าสู่เซลล์สูง รวมถึงสามารถจับกับไมโครอาร์เอ็นเอได้ดีอีกด้วย ดังนั้น อนุภาคไฮดรอกซีแอพาไทต์ที่มี APTES สามารถเป็นระบบนำส่งที่มีประสิทธิภาพเพื่อนำไปประยุกต์ใช้ในการรักษาด้วยไมโครอาร์เอ็นเอ ผลลัพธ์ที่ได้ถือเป็นการเริ่มต้นที่ดีในการพัฒนาระบบการนำส่งไมโครอาร์เอ็นเอด้วยอนุภาคไฮดรอกซีแอพาไทต์เพื่อนำไปใช้ในการเหนี่ยวนำการสร้างกระดูกใหม่ต่อไป

สาขาวิชา	เคมี	ลายมือชื่อนิสิต ....
ปีการศึกษา	2561	ลายมือชื่อ อ.ที่ปรึกษาหลัก ....

5871951623 : MAJOR CHEMISTRY

KEYWORD:

Natthaya Thepphanao :
SYNTHESIS OF HYDROXYAPATITE NANOPARTICLES FOR POLYNUCLEOTIDES
DELIVERY IN DENTISTRY. Advisor: Numpon Insin

Hydroxyapatite (HAp) nanoparticles-based miRNA delivery system has emerged as a promising therapeutic agent for bone regeneration application. In order to achieve high therapeutic performance, the development of HAp functions remains challenging. This study describes the influence of HAp characters on their biological activities with osteoblast cell by synthesized different sizes of rod-like HAp with 150-200 and 100 nm in size and the different shape of elongated particles with 100-150 nm in size. A comparison was carried out on cytotoxicity, cellular uptake, and miRNA binding capacities. The elongated and rod-like shapes of 100-150 nm illustrated the high cell viability, and interestingly, the highest cellular uptake efficiency was observed in elongated particle. However, both particles revealed low ability to condense with miRNA due to their negative surface, the cationic functional molecules, which are APTES and PDMAEMA, were modified on the elongated particle to investigate how surface charge affect their biological properties. The biocompatibility, as well as the high cellular uptake and high miRNA loading efficacies, were noticed in HAp/APTES nanoparticle, which made it possible to be an efficient carrier system for miRNA therapy application. The obtained results could demonstrate a starting point for the development of a HAp-based miRNA delivery system using in bone regeneration application.

Field of Study:	Chemistry	Student's Signature ....
Academic Year:	2018	Advisor's Signature ....

ACKNOWLEDGEMENTS

TABLE OF CONTENTS

Page

LIST OF FIGURES

LIST OF TABLES

LIST OF ABBREVIATIONS

HAp	=	Hydroxyapatite
miRNA	=	microRNA
hMOBs	=	Human mandibular-derived osteoblast cells
APTES	=	3-aminopropyltriethoxysilane
PDMAEMA	=	poly (2-dimethylaminoethyl methacrylate)

จุฬาลงกรณ์มหาวิทยาลัย

CHULALONGKORN UNIVERSITY

CHAPTER 1

INTRODUCTION

1.1. Statement of the problem

Alveolar bone resorption after tooth extraction is a natural phenomenon where the significant bone loss surrounding and supporting the tooth can be observed and ultimately leads to volume and morphological changes of the alveolar ridge. These changes can contribute to many problems in prosthetic dentistry rehabilitation, so many techniques have been applied to prevent residual ridge resorption post-extraction.

Currently, the gold standard for clinical treatments of alveolus defects relies on the application of autologous bone graft, which involves the appropriate load of 'donor' bone harvested from a non-load-bearing site in the patient (especially iliac crest) and transplantation into the defect site.[1, 2] This grafting procedure possesses all the characteristics essential for new bone growth, including (i) osteogenicity (capable of forming new bone directly from osteoblast cells); (ii) osteoinductivity (capable of inducing osteogenic differentiations of local stem cells) and (iii) osteoconductivity (scaffold to permit bone apposition from existing bone).[3, 4] Nevertheless, its use associated with a number of concerns such as limited bone supply, donor site morbidity, risk of rejection and chronic pain.[5] Consequently, synthetic materials for bone repair and regeneration have been developed to overcome the limitations of traditional techniques.

Among numerous materials, hydroxyapatite (HAp) nanoparticle has attracted much attention as an excellent biomaterial in biomedical application, particularly bone regeneration and drug/gene delivery systems, due to its structural and compositional similarity to bone minerals as well as good biocompatibility, biodegradability, osteoinductivity and osteoconductivity properties.[6] Additionally, microRNA (miRNA) has also emerged as an alternative therapeutic option for bone regeneration application due to their ability to regulate the gene expression that can regenerate damaged bone by promoting the biological substitute based on bone cell functions, including cell differentiation, proliferation and apoptosis.[7] Unfortunately, its

susceptibility to nucleases and poor intracellular entry remain the major challenge for using miRNA therapeutics,[8] therefore, HAp nanoparticles can be applied as a carrier system to successfully delivery miRNA into the target cell and concurrently enhance the bone regenerative potential.

Many researches have been made to explore the correlation between HAp characteristics, including particle size, morphology and surface charge, and its abilities for bone regeneration and gene delivery applications. However, the influence of HAp features on the potential as vehicle for miRNA delivery system is not fully appreciated and needs further investigation. This study was hypothesized that it may be possible to optimize the performance of miRNA delivery system on the basis of size, shape and surface charge of HAp nanoparticles. As mentioned, various HAp nanoparticles with different particle size, shape and surface charge were produced to assess their cytotoxicity, cellular uptake efficiency and miRNA binding capacity. These investigations may provide useful information for fundamental design of the HAp nanoparticles for miRNA delivery in bone regeneration application.

1.2. Objectives of this thesis

1. To synthesize and characterize different sizes and morphologies of HAp nanoparticles.

2. To synthesize and characterize HAp nanoparticles with different surface charges by modified with APTES and PDMAEMA polymers.

3. To evaluate the influence of size, morphology and surface charge of unmodified and modified HAp nanoparticles on hMOBs for using as miRNA carrier system.

1.3. Scope of this thesis

This research elucidated the role of particle size, shape and surface charge of hydroxyapatite (HAp) nanoparticles on the efficiency as miRNA delivery system to human mandibular-derived osteoblast cells (hMOBs). For this purpose, a variety of HAp particle sizes and shapes were synthesized via three different approaches: wet chemical precipitation, hydrothermal and reverse microemulsion under hydrothermal

method. The resulted particles were characterized by X-Ray Diffractrometer (XRD), Fourier-Transform Infrared Spectrophotometer (FT-IR), Transmission Electron Microscope (TEM) and Zetasizer. Their biophysical properties, including cellular cytotoxicity, transfection efficiency and miRNA binding capacity on hMOBs were analyzed to find the optimized features of the nanoparticles for using as miRNA carrier system. The suitable material with good biological performance was further functionalized with two positive surfactants: 3-aminopropyltriethoxysilane (APTES) and poly (2-dimethylaminoethyl methacrylate) (PDMAEMA) in order to improve the affinity of the particles with negatively charged miRNA. The characteristics and *in vitro* investigations similar to unmodified HAp experiments were also examined to provide the high-performance miRNA delivery system.

CHAPTER 2

THEORY AND LITERATURE REVIEWS

2.1. Hydroxyapatite nanoparticle (HAp).

Hydroxyapatite (HAp, $Ca_{10}(PO_4)_6(OH)_2$) is the major inorganic constituent of human bone and teeth that belongs to calcium phosphate family with Ca/P molar ratio of 1.67. The most frequently encountered HAp crystal structure is hexagonal with the following crystallographic parameters: a = b = 9.418Å, c = 6.881Å, β = 120°. The crystalline network of the stoichiometric HAP can be described in Figure 2.1, an array of tetrahedral PO_4 groups, where P^{5+} ions are in the center, of which the tops are occupied by 4 oxygen atoms surrounded by octahedral Ca^{2+} ions interspersed among them. The Ca ions are founded in two different sites, in accurately aligned columns, denoted Ca(I) (4 per a unit cell) and in peripheries, referred to as Ca(II) (6 per a unit cell), and the adjacent OH⁻ groups point in opposite directions to balance the positive charge of the matrix. [9]
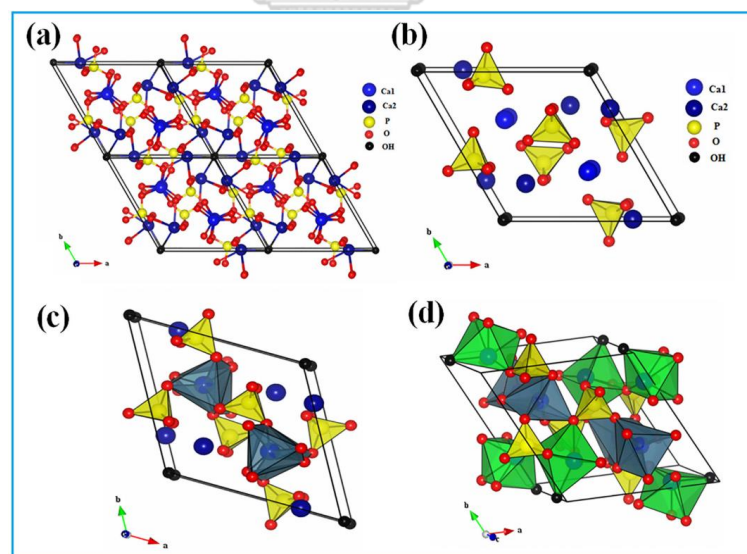
Figure 2.1. a) The HAP unit cell along the (001) plan; (b) projection of octahedrons [Ca(I)] ; (c) octahedral [Ca(I)] and tetrahedral [PO₄] arrangement; and (d) octahedral of [Ca(I)] and [Ca(II)], and tetrahedral [PO₄] arrangement in the HAp structure.[10]

Recently, nanometer-scale form of HAP has been attracting increasing attention due to its many excellent features such as a good bioactivity and biocompatibility properties with respect to bone cells and other body tissue. Furthermore, it also holds a good osteogenesis, osteoinductivity and osteoconductivity abilities which are important in bone remodeling process where bone tissue is simultaneously created by the bone cells (osteoblast).[11] Additionally, it can degrade into ions in all cells, which makes it a safe intracellular delivery carrier for the therapeutic small molecules and genes. Despite of these characteristics, it also possesses high binding affinity to negatively charged nucleic acids via positively charged calcium ion and is consequently protected from degradation by endonucleases.[12] Benefiting from its favorable properties, therefore, HAp nanoparticles has been considered as an important biomaterial for use in medical and dental applications, including tissue engineering, implant coating and especially in gene delivery system.

2.2. MicroRNA (miRNA).

MicroRNA (miRNA) represents a major class of small non-coding RNAs which is a single-stranded RNA approximately 21-25 ribonucleotides in length that is found in many plants, animals and viruses.[13] Basically, biogenesis of miRNA involves a multi-step processes that occurs through a mechanism known as RNA interference (RNAi) pathway (Figure 2.2). This pathway is initiated with the transcription of miRNA genes to a primary miRNA (pri-miRNA) by RNA polymerase II or RNA polymerase III and is then processed to a short precursor miRNA as pre-miRNA by the action of ribonuclease, Drosha. Afterward, the pre-miRNA is exported to the cytoplasm by Exportin-5 (Exp-5). In the cytoplasm, it is further transformed to the mature miRNA by an RNAse III endonuclease called Dicer and incorporates into the effector complex RNA-induced silencing complex (RISC). This miRNA generally binds to the target messenger RNA (mRNA) resulting in translation inhibition by cleavage of target mRNA which leads to prevention of protein production and thereby functioning as gene expression silencing.[14, 15]
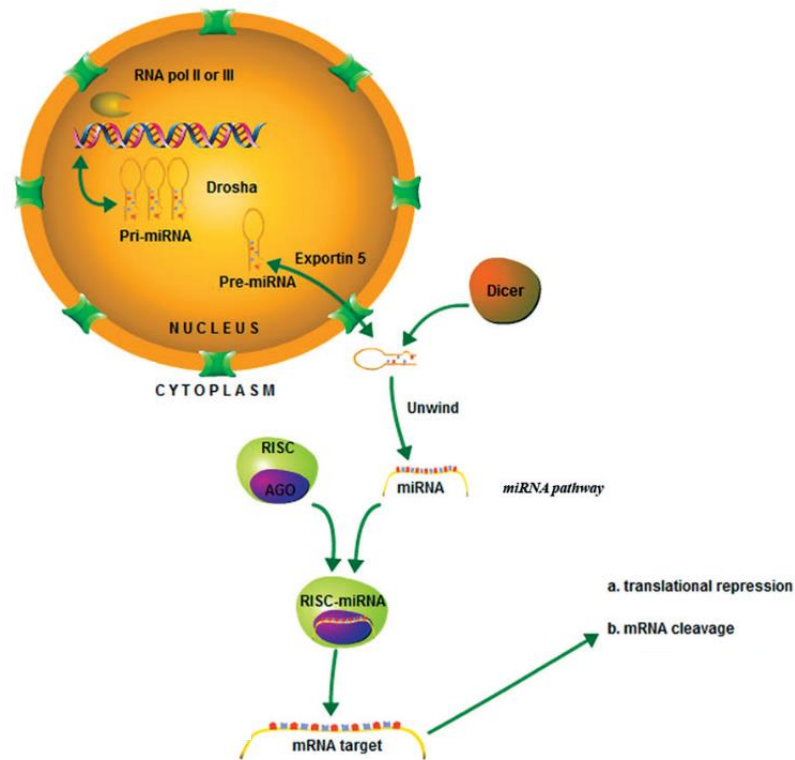
Figure 2.2. The RNA interference pathway of miRNAs.[14]

As described before, miRNA has revealed the potential regulating roles in the expression of the gene. This action can affect diverse cellular processes, including cell differentiation, proliferation, progression and apoptosis[16]. As a result, development of miRNA as a therapeutic molecule in gene therapy are increasing steadily for treatment of various diseases and abnormal change in gene functions.

Despite its several advantages in biomedical applications, miRNA still has the major limitations in its efficient delivering to the target cells. In most cases, naked miRNA can be degraded within seconds by the endonucleases before achieving target manipulation and cannot escape from the endosome.[12, 17] Therefore, a suitable carrier agent is required to protect miRNA from biological environment and facilitate the intracellular uptake and endosomal escape.

2.3. Principal methods for synthesis of HAp.

The crystallinity, size and morphology of HAp play an important role in showing their biological properties in biomedical applications. Many synthesis approaches have

been reported for the production of HAp with various features; however, processing conditions and reagents vary widely for each method. Herein, the synthetic methods are divided into three techniques: i) wet chemical precipitation, ii) hydrothermal and iii) emulsion method.

2.3.1. Wet chemical precipitation method.

Wet chemical precipitation or co-precipitation is the most commonly used method for the preparation of HAp owing to its several advantages such as high purity yield, simplest procedure, low reaction temperature and cost-effectiveness.[18] This technique is typically involved the reaction between aqueous solution of calcium precursor and phosphate precursor at the Ca/P molar ratio of 1.67 by dropwise addition of one reagent to another under continuous and gentle stirring, followed by aging to complete the reaction. The conditions for this process are variable based on the fact that at room temperature and pH 4.2, HAp is the least soluble and the most stable calcium phosphate phase in an aqueous solution. However, generally the precipitation reaction is carried out at higher pH values ranging from 4.2 to 12 and at temperature ranging from room temperature to temperature close to the boiling point of water in order to increase reaction rate and product crystallinity.[19] Therefore, the pH value of solution must be kept constant to precipitated HAp particles by addition of other additives (base or acid). Some research claim that adjustment of pH value by the addition of ammonium solution (NH_4OH) provides more homogeneous precipitation and drives the phase transformation to HAp according to this equation.[20]

$$10Ca^{2+} + 6PO_4^{3-} + 2OH^- \longrightarrow Ca_{10}(PO_4)_6(OH)_2$$
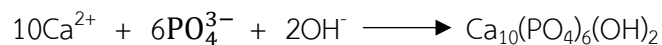
Besides other parameters, the reaction is sometimes performed in the presence of templates such as CTAB and ethanolamine with the aim at controlling the growth direction and results in desired characteristics of final powder products.

2.3.2. Hydrothermal method.

Hydrothermal technique, as one of efficient means for the synthesis of HAp, is simply identified as a wet chemical precipitation which is performed in the presence of a supercritical solvent (whether aqueous or nonaqueous) at high pressure above 1 atm and temperature above 100 °C inside an autoclave or a pressure vessel.[20] The formation of HAp crystals usually occurs through two main steps which can be illustrated in Figure 2.3: (i) nucleation step of tiny crystalline nuclei in a supersaturated medium (reaction of ions) and (ii) growth step of nuclei into the final shape and size (hydrothermal treatment).[21]
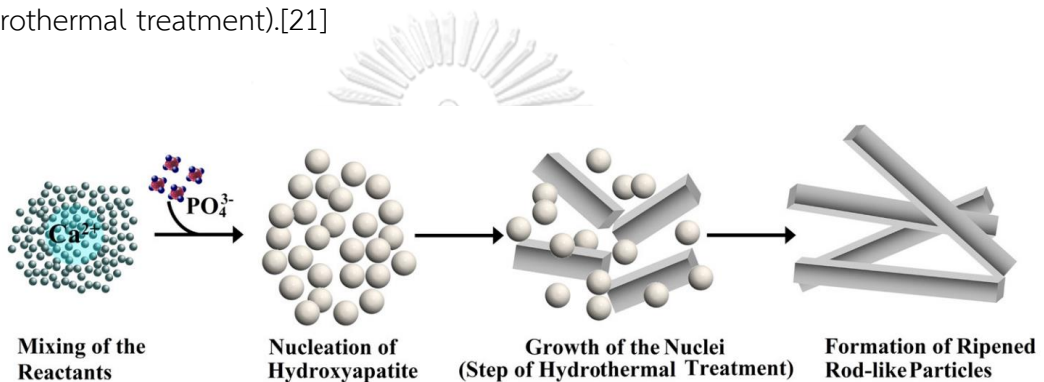
Figure 2.3. The formation of HAp into rod-like shape.

This process enables the synthesis of homogeneous HAp with high crystallinity and high aspect ratio close to the stoichiometric value.[22] However, the most notable drawback of this method is the poor ability to control the morphology and size distribution of nanoparticles which usually yield agglomerated HAp crystals.[23] Many researchers reported that pH value are the important factor, which directly affects the structural and morphological properties of HAp. It was found that an increased pH values to ~10-12 leads to an isotropic growth to form sphere or short rod-like shape; in contrast, lower pH values to ~4-6 leads to an anisotropic growth to form rod-like or plate shape.[19] Same as co-precipitation, a number of templates such as EDTA and oleic acid are utilized to control the shape and improve size distribution of HAp particles.

2.3.3. Emulsion method.

Emulsion method has been considered to be a promising technique that is able to provide HAp particle size in the range of nanometers, together with minimizing particle agglomeration and controlling the morphology.[24] In addition, it is also simplicity and can be prepared under mild synthesis condition.

A microemulsion is a heterogeneous system which consists of a stable colloid disperse in two immiscible liquids, for example, oil and water stabilized by the amphiphilic surfactant (e.g. CTAB and triton X-100) and co-surfactant. Addition of a surfactant, a molecule composed of hydrophilic and a hydrophobic part, is required to decrease interfacial tension between the two immiscible phases, resulting in a nano-dispersed phase with diverse organized assemblies such as spheres and rods, which strongly depends on the type and concentration of surfactant and the liquid medium phases.[25] The restricted space of these assemblies provides an appropriate environment for the controlled nucleation/growth of the crystals. Moreover, cosurfactants are often used to enhance the stability and the solubility of microemulsion.[26]

The emulsion method can be conducted via three major systems, including oil-in-water system, water-in-oil system, and water-in-oil-in-water system.[19] The process of these systems is demonstrated in Figure 2.4. However, the water-in-oil system is accounted as the most widely used method for synthesis of HAp nanoparticles. In the case of water-in-oil emulsion, a transparent solution containing reverse micelles of aqueous phase suspending in a continuous nonaqueous phase is formed. Each micelle comprises a core aqueous phase surrounded by a monolayer of amphiphilic surfactant molecules, which is normally called "water pool". Brownian motion of reverse micelles causes the fusion–fission process between the reverse micelles, followed by the reaction of reactant ions in aqueous phase and ultimately formation of HAp particles, as demonstrated in Figure 2.5.[27] The conditions of the emulsion system can be adjusted to obtain a different morphology and particle size of HAp particles.
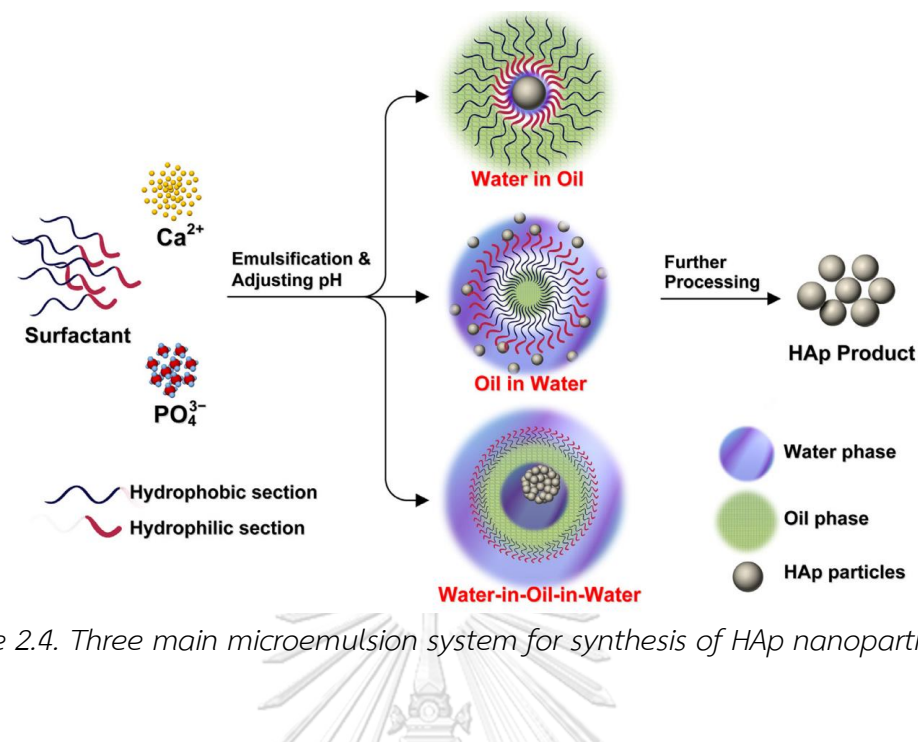
Figure 2.4. Three main microemulsion system for synthesis of HAp nanoparticles.[19]
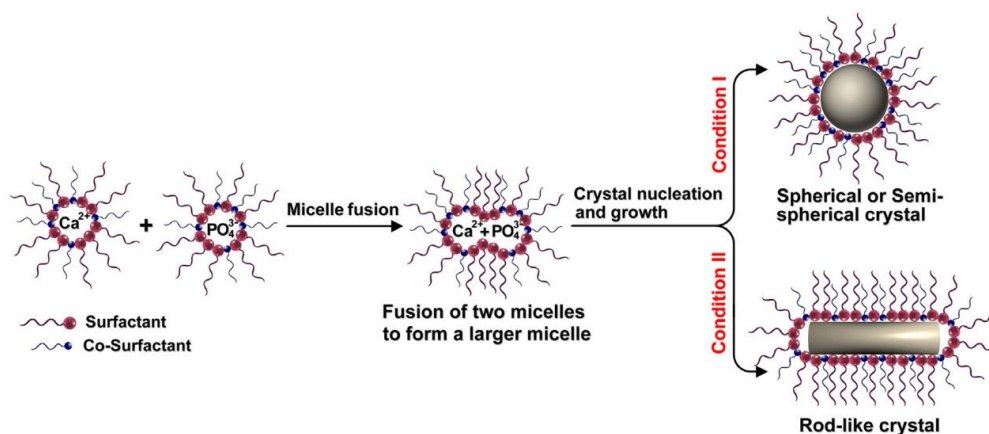
Figure 2.5. Fusion–fission mechanism of the reverse microemulsions of reactant to produce HAp nanoparticles in sphere or rod shape.[19]

However, the HAp nanoparticle remains brittleness that could limit their applications to bear the load. In order to expand its properties, HAp has been functionalized with diverse polymers [2–4] such as poly (lactide-co-glycolide) (PLGA), poly(L-lactide) (PLLA) and collagen to take an advantage of polymers and therefore illustrate the bright prospects for bone regeneration application.

2.4. Bone remodeling process.

Bone remodeling is a continuous metabolic process of bone throughout life that occurs to replace old bone with newly formed bone, repair damage bone due to daily physical load and secure systemic mineral homeostasis by liberating stores of calcium and phosphorus in order to maintain bone structural integrity.[28] This process relies on the activities of two principal cell types of the bone tissue which are:

- Bone-resorbing osteoclast is a giant multinucleated cell formed from the fusion of the monocyte/macrophage mononuclear which originates from hematopoietic stem cells.[29] It is responsible for the resorption of the bone matrix by secreting hydrochloric acid to dissolve the inorganic component (mainly hydroxyapatite) and proteolytic enzymes to subsequent digest organic component of the bone matrix encapsulated within the sealing zone.[30]

- Bone-forming osteoblast is a cell that derived from mesenchymal stem cells in the bone marrow and is responsible for the production of the bone matrix by secreting protein (mainly Type I collagen) and subsequent mineralization of hydroxyapatite deposit.[31] The osteoblast has completed its bone-forming function by differentiation into three possible fates as illustrated in Figure 2.6; they can be embedded in bone matrix as osteocytes, formed clusters cover the bone surface as lining cells, or undergo apoptosis.[32]

Indeed, the osteocyte is also considered as an important cell that involve in the bone remodeling cycle by act as a mechanosensor that provides the signal for regulating the action of osteoclast and osteoblast response to mechanical forces such as impact loading.[33]
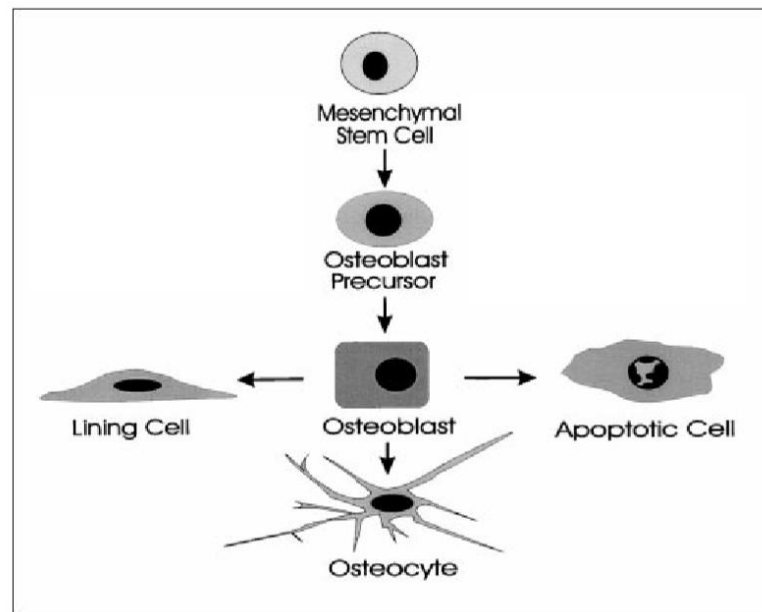
Figure 2.6. The differentiation pathways for osteoblast.[33]

The balance functions between bone resorption by osteoclasts and bone formation by osteoblasts that are tightly coupled both spatially and temporally have been proposed to maintain normal physiological bone remodeling.[34] This process is accomplished according to the five consecutive phases as illustrated in Figure 2.7.

1. Activation phase. Different events, for example, mechanical loading, microfracture detected by the osteocytes or some systemic changes such as parathyroid hormone (PTH), activate the surface expression of RANKL (receptor activator of nuclear factor kappa-B ligand) on the lining cells. This ligand further binds to its respective receptor on the pre-osteoclasts, receptor activator of nuclear factor kappa-B (RANK), resulting in the initiation of pre-osteoclast differentiation toward multinucleated osteoclasts.[35]

2. Resorption phase. Once differentiated, the osteoclasts polarize by rearrangement of the cytoskeleton for adhesion to the bone surface and formation of a sealing zone that separate the bone resorption area from the rest of the environment. Within the sealed compartment, the osteoclasts begin to dissolve bone in two steps: (i) demineralization of the inorganic component by acidification, exposing collagen within and (ii) degradation of the organic component (collagen-rich bone) by

proteolytic enzymes. The resorption phase is terminated by osteoclasts undergoing apoptosis to avoid an excessive bone resorption.[36]

3. Reverse phase. This phase is not yet fully understood. However, it is known that there are mononuclear cells as macrophage with a function of removal the debris produced during bone degradation from the resorption cavity.

4. Formation phase. Bone matrix resorption promotes the release of several growth factors that leads to the recruitment of the osteoblasts into the reabsorbed area. The osteoblasts produce the new bone matrix to fill the cavity via two steps: (i) synthesis of Type I collagen-rich bone matrix (osteoid) and (ii) regulating its mineralization whereby hydroxyapatite crystals are deposited around collagen fibrils.

5. Termination phase. Once formation phase is complete, some osteoblasts change into bone-lining cells or undergo apoptosis whilst others become trapped within the bone matrix and ultimately differentiate into osteocytes. Osteocytes play an important role in signaling the end of bone remodeling cycle by releasing the antagonists to stop osteogenesis.[37]
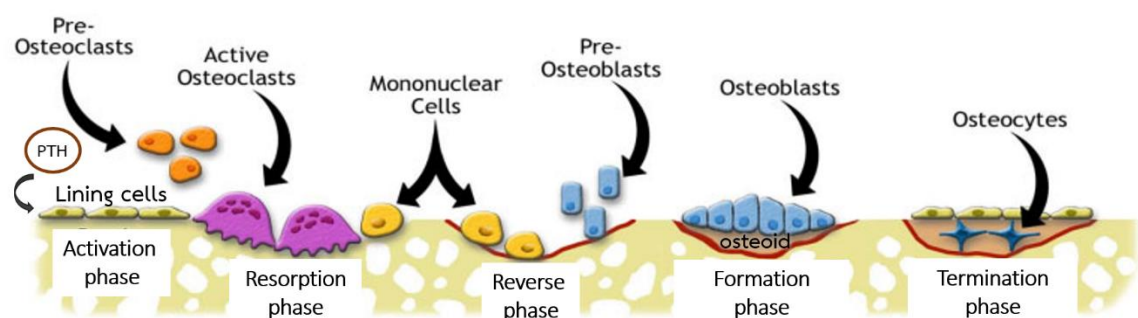
Figure 2.7. The bone remodeling process.[38]

Abnormalities of the bone remodeling cycle or imbalance between bone resorption and formation process often results in the progression to various bone pathologies, most commonly bone loss and osteoporosis. These diseases are

characterized by low bone mass, as a result of a decreased bone formation by osteoblast function and/or enhanced bone breakdown by osteoclast activity.[39]

Based on a better understanding of bone remodeling mechanism, the potential therapeutic agents that promote the differentiation, proliferation and development of osteoblast has been considered as one of crucial approaches for treatment of bone loss and osteoporosis.

2.5. Literature reviews.

Hydroxyapatite (HAp), a calcium phosphate with chemical formula similar to bone and teeth composition, is a suitable material for a broad range of biomedical applications, particularly those relating to bone and teeth, because of its predominant characters as mentioned above. Numerous researches are nowadays involved in the development of biomaterials based on HAp nanoparticles for applications in the biomedical field of bone and teeth.

For example, Uskoković *et al.[40]* focused on the comparative effect of four morphologically different calcium phosphate particles: monetite (plate-shaped and elongated orthogonal), octacalcium phosphate (brick-shaped), and hydroxyapatite (spherical) (Figure 2.8a) on osteogenic and antibiotic delivery properties for treatment of osteomyelitis. They have come to conclusion that the hydroxyapatite with the average particle dimension of 20 nm spherical particle exhibited satisfying osteogenic and antibacterial potency compared to other calcium phosphate phases with different morphologies. The highest gene expression upregulation of three osteogenic markers (BGLAP, Runx2, and BSP-1), key factors for osteoblast differentiation, in osteoblastic MC3T3-E1 cells (Figure 2.8c) as well as the most effective bacterial growth inhibition (Figure 2.8b) were observed for the spherical hydroxyapatite nanoparticles.
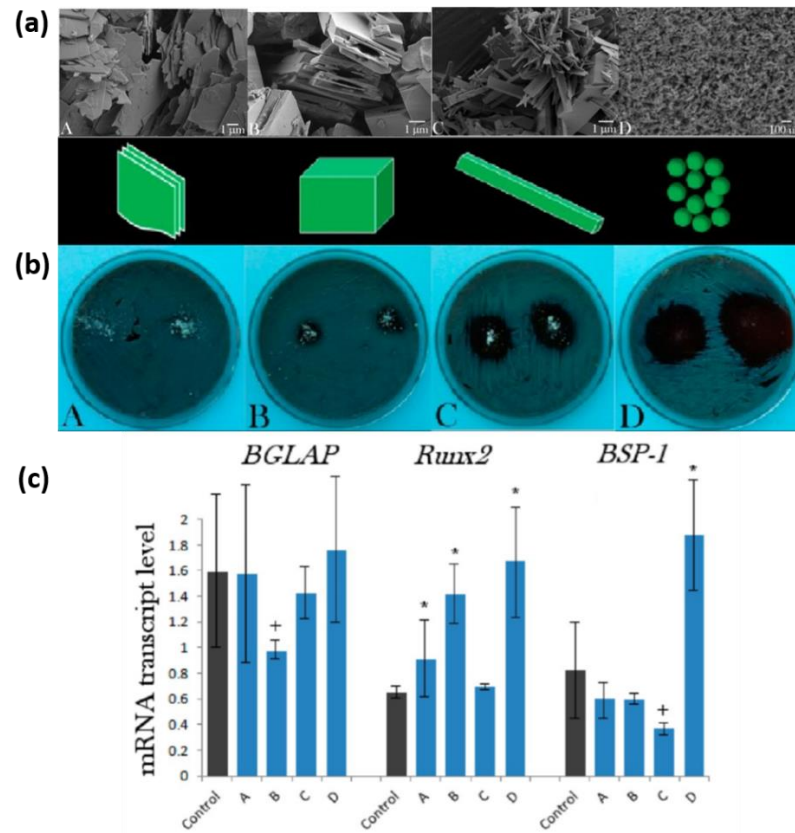
Figure 2.8. (a) SEM images of the calcium phosphate particles, (b) Bacterial growth inhibition testing of antibiotic-loaded calcium phosphate particles, (c) The mRNA expression levels of three osteogenic markers: BGLAP, Runx2, and BSP-1 in osteoblastic MC3T3-E1 cells for (A) plate-shaped monetite, (B) brick-shaped octacalcium phosphate, (C) elongated orthogonal monetite and (D) spherical hydroxyapatite. * and + at p < 0.05 of significantly upregulated and downregulated comparison with the control group, respectively.[40]

The excellent properties of HAp for biomedical applications of bone and teeth were also confirmed by Hoai *et al.[41]* They synthesized rod-like shaped HAp nanoparticles with average size of 39 nm in width and 125 in length by the hydrothermal approach using CTAB as a surfactant. The research demonstrated that the HAP nanorods revealed highly biomineralization capability by rapid forming a bone-like mineral layer (Ca/P=1.58) after immersing in simulated body fluid (SBF) for 7 days as indicated in Figure 2.9. The obtained results support a potential application of HAp nanoparticles for use in bone repair and regeneration.
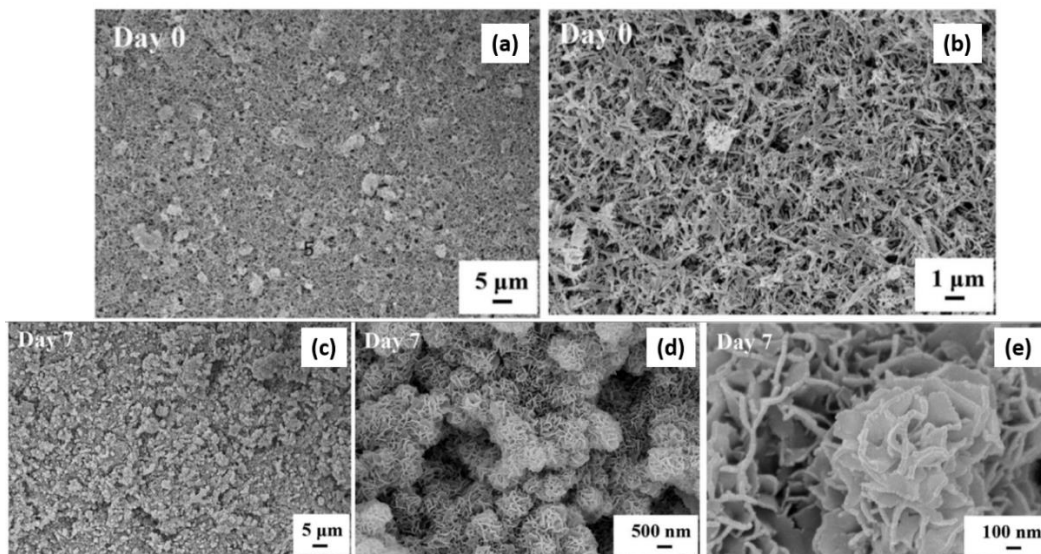
Figure 2.9. FE-SEM images of (a, b) HAp nanorods on poly-d,l-lactic acid (PDLLA) films before addition of SBF at 1k and 5k, respectively and (c, d, e) Mineral deposition on the film after 7 days addition of SBF at 1k, 10k, and 50k, respectively.[41]

Alternatively, miRNA has also received an increasing attention as therapeutics in biomedical applications of bone and teeth by regulating the gene expression of target cells that leads to cell differentiate, development and apoptosis. Recent literatures highlighted regulatory roles of miRNAs in various cellular processes, particularly in bone regeneration.

According to Lin *et al.*,[42] they demonstrated that miR-92a-1-5p was identified as a negative regulator in osteogenic differentiation of MC3T3-E1 cells by downregulation of the translational and transcriptional levels of β-catenin which acts as a promoter in osteogenic differentiation. Consequently, this finding offered new pathway in the possibility of miR-92a-1-5p function as a promising therapeutic for management of bone regeneration.

In contrast, Yang *et al.[43]* suggested that miRNA-21 play an essential role as a positive regulator in osteogenic differentiation of bone marrow-derived stem cells (BMSCs) by increasing P-Akt and HIF-1α activation, known as important markers of osteoblast differentiation, thereby promoting bone regeneration in bone defect. The

results indicated that miRNA-21 overexpression in BMSCs provided an effective therapeutic for bone defect reconstruction.

miRNA therapy, therefore, is considered as a potential therapeutic paradigm for diverse biomedical applications. However, the major challenge of miRNA therapy is insufficient delivering the miRNA into the target cell that contributes to the need of suitable miRNA delivery system.

To overcome this limitation, HAp has showed as a biomaterial to be a miRNA carrier in gene delivery system. Owing to the miRNA binding ability as mentioned above, HAp is able to encapsulate miRNA and protect it from biological environment and then dissolves in the acidic pH within endosomes and lysosomes leading to the release of miRNA in the targeted region of the cells. Therefore, miRNA-based therapeutic agent loaded into HAp might offer a new strategy for a successful miRNA delivery system for biomedical applications.

The successful combination of desired properties of HAp nanoparticles and miRNA was studied by Castaño *et al.[44]* They developed the miRNA delivery system using HAp nanoparticles to deliver the therapeutic miR-133a inhibitor (antagomiR-133a), a direct positive regulator of the osteogenesis factor (Runx2), based on collagen-nanohydroxyapatite scaffold as could be seen in Figure 2.10b. This system revealed enhanced osteogenesis in human bone marrow mesenchymal stem cells (hMSCs) by directly upregulating the miRNA level of Runx2 (Figure 2.10c). Thus, this platform based on HAp nanoparticles can be served as a potential agent for miRNA delivery to trigger enhanced functional osteogenesis in fields of bone regeneration application.
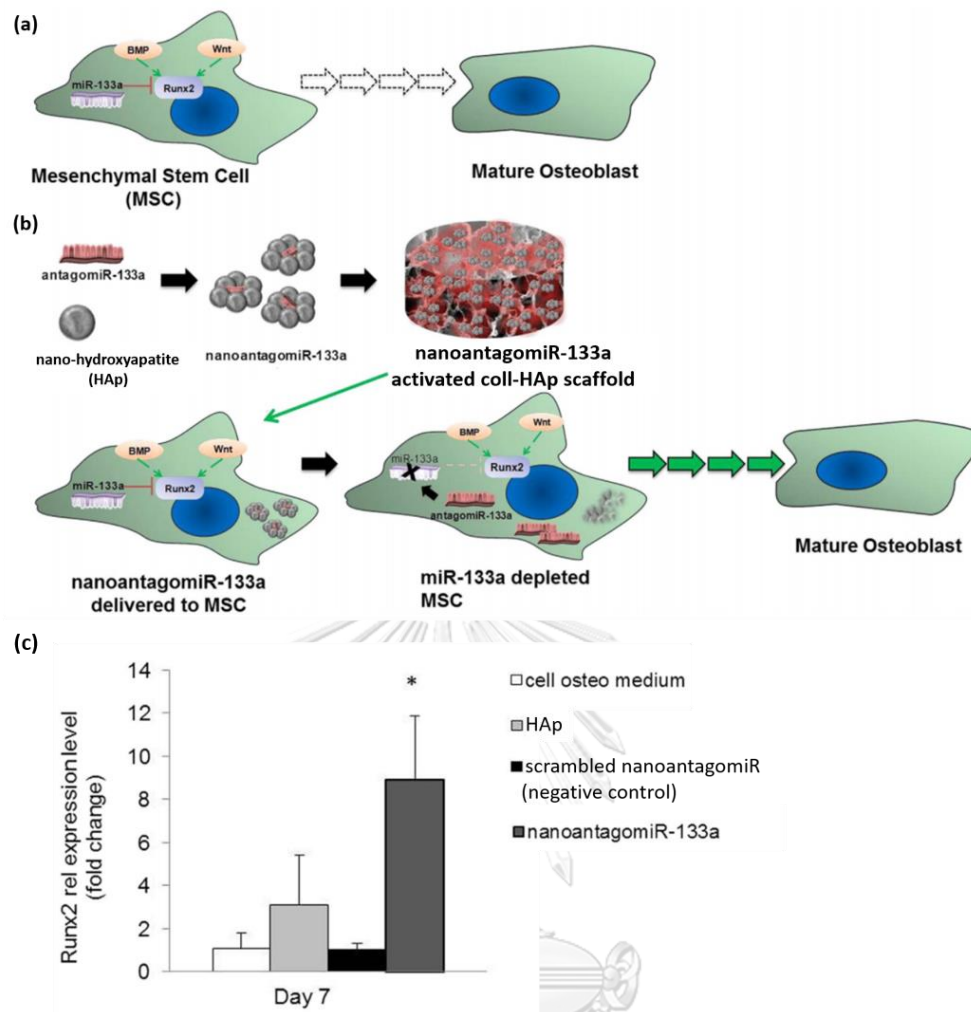
Figure 2.10. Role of antagomiR-133a in osteogenesis of mesenchymal stem cell
(MSC). (a) miR-133a downregulate the Runt-related transcription factor 2 (Runx2)
(red line) that suppresses initiate differentiation towards a mature osteoblast state.
(b) AntagomiR-133a forms complexes with HAp nanoparticles which are
incorporated in collagen-HAp scaffolds and functions by inhibiting miR-133a (black
line), decreasing the suppression of Runx2 (faded red line), that leads to higher
expression of Runx2 which promotes osteogenesis of MSCs to maturity stage. (c)
Runx2 expression after treatment with nanoantagomiR-133a for 7 days. Mean ± SD
(n=4). * Significantly different, $p < 0.05$.[44]

Due to various size, shape and surface charge of HAp nanoparticles, their
properties can be an important factor for considering in the biomedical applications in
bone and the miRNA delivery efficiency. As previously reported, Yang et al.[45]

exhibited that the different-sized HAp nanorods in length of ~50, ~100, and ~150 nm (Figure 2.11a) had stimulatory effect on the osteogenic differentiation of human bone marrow mesenchymal stem cells (hMSCs). Comparison between the three different sizes, HAp with smaller-sized nanorod (~50 and ~100 nm) possess high effective in enhancing expression of osteogenic related markers (ALP, OPN, Runx2, and OCN) as shown in Figure 2.11b, resulting in higher stimulating osteogenic differentiation of hMSCs. These suggest that HAp nanorod with ~50 and ~100 nm in size can be a good reference for using HAp in bone regeneration applications.
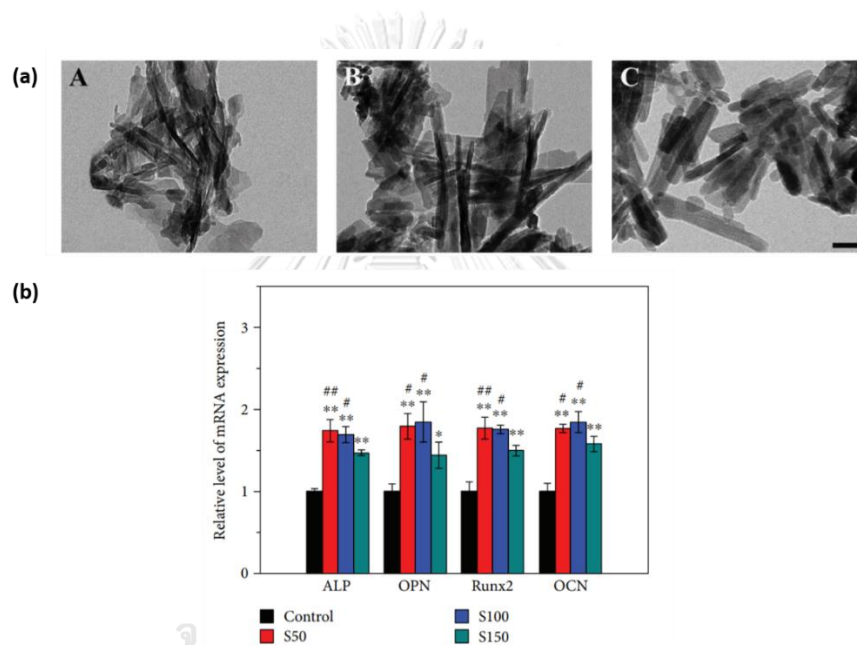
Figure 2.11. (a) TEM images of HAp nanoparticles in length of (A) 50, (B) 100, and (C) 150 nm. The bar is 50 nm. (b) mRNA expression levels of four osteogenic markers after 14 days incubation. Data are represented as mean ± SD (n = 3). Significantly different at *p < 0.05, **p < 0.01 comparison to the control group (untreated HAp). #p < 0.05, ##p < 0.01 compared between different size of HAp nanoparticles.[45]

Furthermore, Shi *et al.*[46] also provides an interesting view of the role of HAp sizes on biomedical applications. They claimed that HAp nanosphere with diameter of 20 nm (np20) has the most effectiveness at promoting cell growth and inhibiting cell apoptosis on human osteoblast-like MG-63 cells compared to the nanostructures of spherical-like, 80 nm (np80) and rod-like, width of 30–80 nm and length of 200–500

nm (m-HAp) as displayed in Figure 2.12. Their study suggested that HAp nanosphere with average diameter of 20 nm could be an ideal biomedical material in biomedical applications.
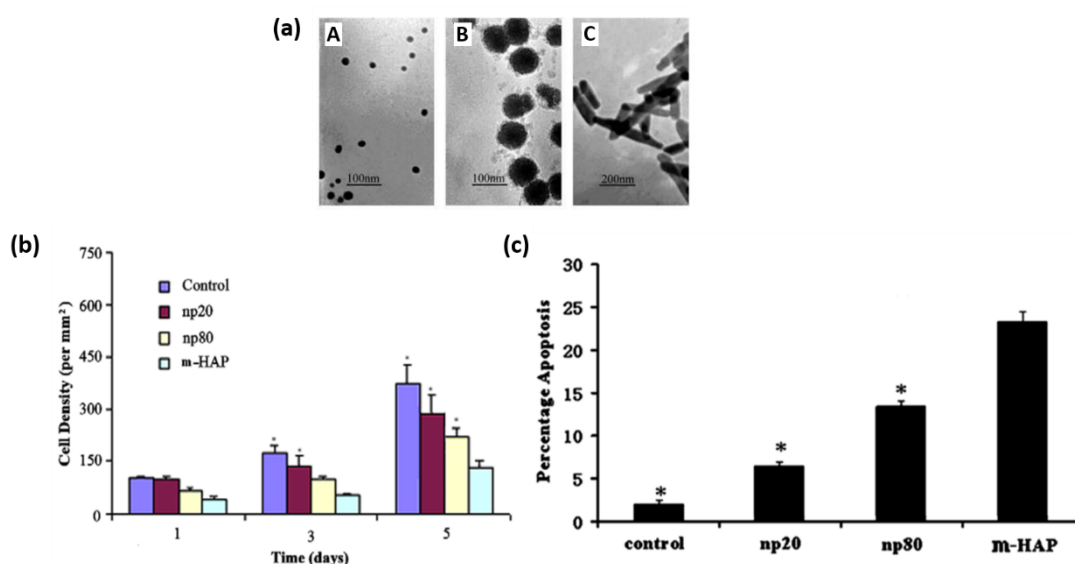
Figure 2.12. (a) TEM images of spherical HAp in size of (A) 20, (B) 80 nm and (C) rod-like HAp. (b) MG-63 cell density in different particle sizes for 1, 3 and 5 days. (c) Cell apoptosis of MG-63 in different HAp sizes for 5 days. Data are presented as mean values ± SD (n = 6), * Significant different compared to m-HAp at p < 0.05.[46]

The morphology of HAp particles is another important factor that has great influence on their biological properties. For example, Huang *et al.*[47] prepared different morphologies of HAp with nanorods, flake-like and dandelion-like shapes represented in Figure 2.13A by a hydrothermal process using cetyltrimethyl ammonium bromide (CTAB), ammonium tartrate (AT) and trisodium citrate (TSC) as soft templates, respectively. They suggested that the rough surface of material has more beneficial for cell adhesion and proliferation than others. It was found that osteoblast cell proliferation on the rod-like HAp morphology was better than on the flake-like and dandelion-like morphology, which was observed from the gradually increased optical density (OD) in CCK-8 assay (Figure 2.13B). The result indicated that rod-like HAp nanoparticles might be an optimal morphology for potential biomedical applications.
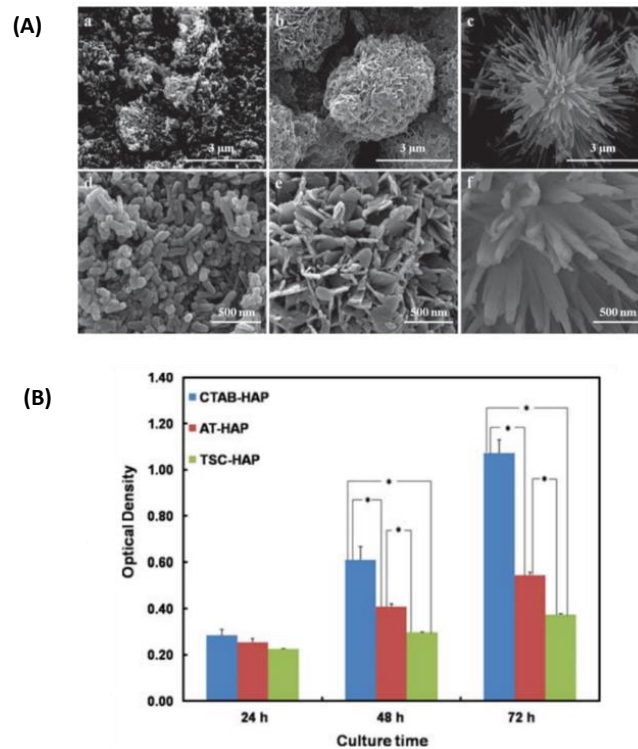
Figure 2.13. (A) SEM images of the surface topography of the HAP synthesized using different templates: (a, d) rod-like (b, e) flake-like (c, f) dandelion-like. (B) CCK-8 assay of osteoblasts incubated on CTAB-HAP, AT-HAP and TSC-HAP from 1 to 3 days for cell proliferation. Significant difference in the 48 h and 72 h (*p < 0.05, n = 3).[47]

Besides particle size and morphology, previous studies have provided evidence that the surface charge of HAp particles also affects the bone cell behavior. From Chen *et al.* research,[48] they proposed the influence of surface charges of HAp on the intracellular uptake, cell viability and proliferation of osteoblast cells (MC3T3-E1) by functionalization with similar carboxylic acid compounds to minimum interference from other factors: 12-aminododecanoic acid (amine group on side chain, positive charge), dodecanedioic acid (carboxyl group on side chain, negative charge) and dodecanoic acid (methyl group, neutral) as demonstrated in Figure 2.14A. TEM images (Figure 2.14B) exhibited that the positively charged HAp nanoparticles could be more easily penetrate into osteoblast cells because of the attraction force with the negative charge of cell membrane. In addition, MTT and LDH assay (Figure 2.14C, D) revealed that the highest cell proliferation and concurrently less cytotoxicity were also obtained

from the positively charged HAp nanoparticles as well. Consequently, the positive charge of HAp nanoparticles is promising for the biomedical applications because of its high cellular uptake and biocompatibility.
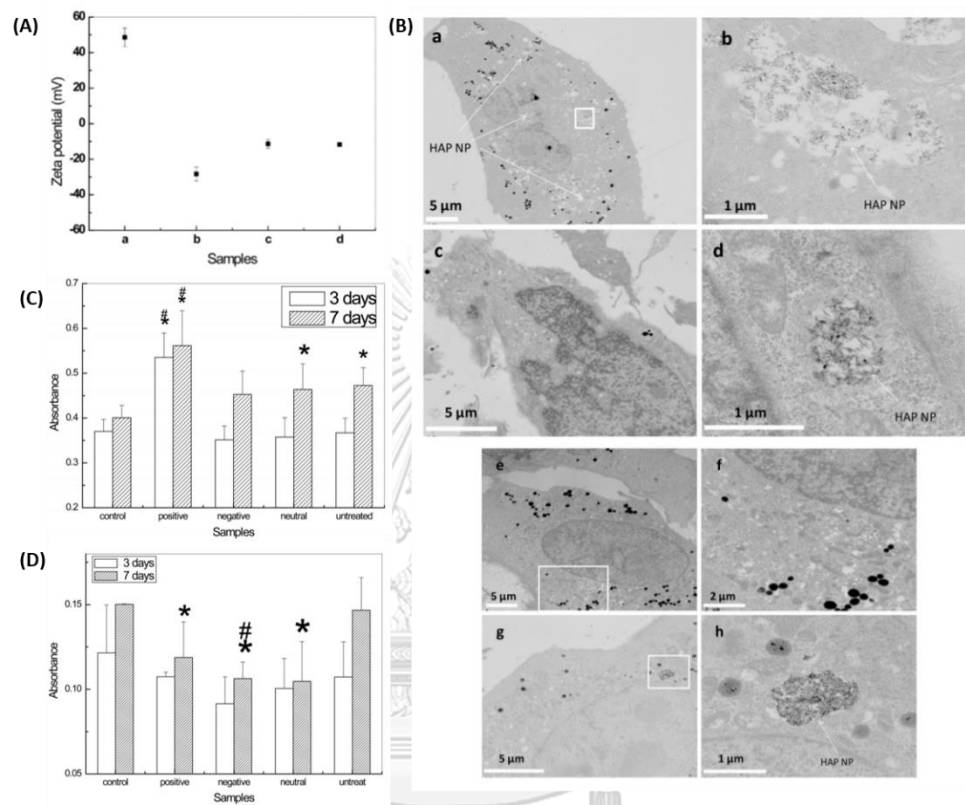
*Figure 2.14. (A) Zeta potential of the modified HAp nanoparticles with: positive charge of (a) 12-aminododecanoic, negative charge of (b) dodecanedioic acid, neutral of (c) dodecanoic acid and (d) unmodified, in PBS solution at pH value of 7.4. (B) TEM images of osteoblast cell incubated in: (a, b) positive charge, (c, d) negative charge, (e, f) neutral, (g, h) unmodified. The right images present an enlarged square area of the left image. (C) The proliferation and (D) cytotoxicity of MC3T3-E1 cell after incubation with different surface charge of HAp nanoparticles by MTT and LDH assay, respectively. Data are shown as the mean±SD (n=5). *Significant difference at P<0.05 compared to controls, #P<0.05 compared to unmodified HAp.[48]*

Many researchers also attempt to provide a broad overview of the influence of particle size, morphology and surface charge of HAp nanoparticles on capability as gene delivery system. Bakan *et al.[49]* reported the comparison on siRNA binding capacity of a various siRNA delivery systems using chemically and morphologically different calcium phosphate (CaP) nanoparticles: spherical-like hydroxyapatite (HA-s), needle-like hydroxyapatite (HA-n) and calcium deficient hydroxyapatite (CDHA) nanoparticles as illustrated in Figure 2.15a, followed by functionalized the particle with cationic amino acid (arginine) to investigate the influence of surface charge on their properties. It can be seen in Figure 2.15c that arginine functionalized HA-n nanoparticles has the best siRNA loading capacity due to their high positive zeta potential of +18.8 mV (Figure 2.15b). The results suggested that high siRNA entrapment in arginine modified HA-n nanoparticles can be a potential carrier system for gene therapy.
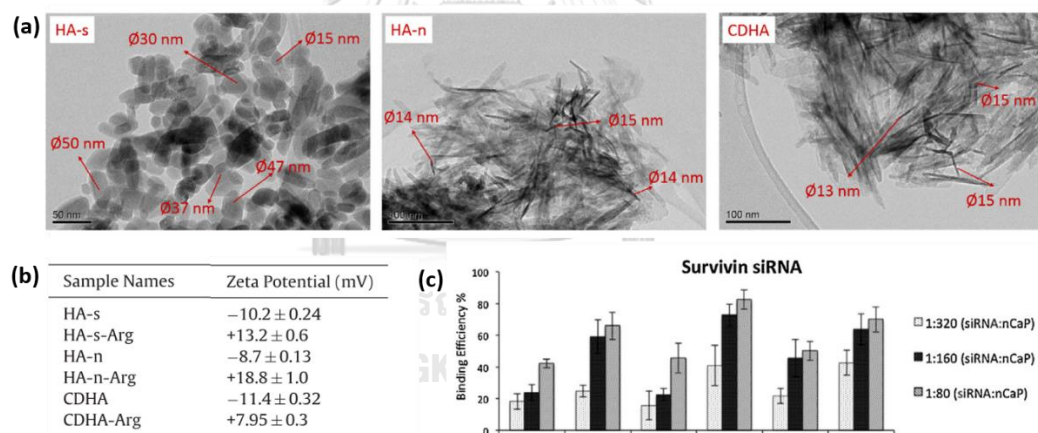
Figure 2.15. (a) TEM images of different CaP nanoparticles. (b) Zeta potential values of nanoparticles. (c) siRNA binding capacities of CaP nanoparticles. Data represent mean ± SD, (n = 3).[49]

Additionally, Cai *et al.[50]* also presented the ability of HAp characters to control the efficiency of gene delivery system. They provided the alteration in the HAp surface charge by functionalized the particle with different lengths of cationic poly (2-dimethyl amino) ethyl methacrylate (PDMAEMA) chains, including HA-PDM1, HA-PDM2, and HA-PDM3 with average polymer's molecular weight of 9.6 x 10^3, 1.4 x 10^4 and 2.3

x 10^4 gmol^{-1}, respectively. In comparison, the HA-PDM possessed increasing plasmid DNA (pDNA) binding ability with the increased positive groups of the polymer chains as observed in the retarding of pDNA migration by agarose gel electrophoresis (Figure 2.16a). The HA-PDM2/pDNA complex also could largely enhance the osteogenic differentiation of osteoblast MC3T3 cells as illustrated in the increasing of alkaline phosphatase (ALP) activity, an indicator of the osteogenesis (Figure 2.16b). Interestingly, the PDMAEMA grafted HA has obviously higher performance than polyethyleneimine (PEI) carrier, although PEI is regarded as the gold standard gene delivery agent because of its high transfection efficiency. Therefore, PDMAEMA functionalized HA nanoparticles is an effectively-designed approach for act as a carrier of therapeutic agent in biomedical applications.
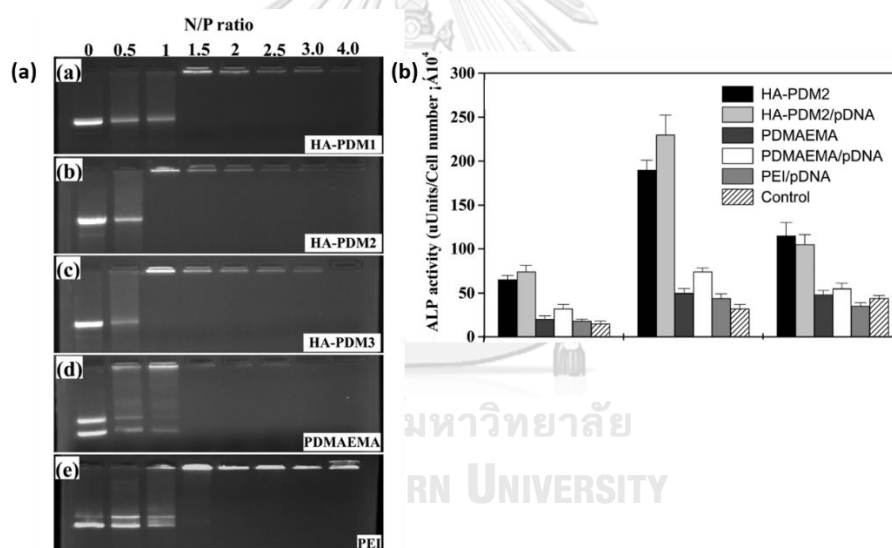
Figure 2.16. gel electrophoresis of pDNA in the different complexes at various ratios of nitrogen in modified HAp (N) to phosphate in pDNA (P). (b) ALP activity of MC3T3 cells of different carriers. Data are presented as means ± standard deviation (n = 3).[50]

Considering the above results, HAp nanoparticles and miRNA were confirmed to be a potential biomaterial for biomedical applications, especially in bone and teeth. These data also provided improved understanding of the correlation between diverse HAp characteristics, including particle size, morphology and surface charge, and

functional properties of HAP nanoparticles in bone regeneration and gene delivery system. HAp nanoparticles with the size range of 20-100 nm and the morphology varied from spherical-like, rod-like and needle-like shapes with positive surface charge are believed to demonstrate more effective biological properties. However, the investigations based on HAp features remain unclear whether it holds a similar performance for miRNA delivery system.

In this research, the former studies were expanded with the aim at optimizing the HAp characters for using as a miRNA delivery carrier by synthesizing different sizes and morphologies of HAp particles, followed by modifying with positive functional molecules to obtain a variety of surface charge. Their properties were then elucidated by subjecting them to analyses of their (a) cell viability; (b) cellular uptake efficiency; and (c) miRNA loading capacity on human mandibular-derived osteoblast cells (hMOBs) *in vitro*. The results will be expected to play a guiding significance in the design of HAp particles for biomedical applications.
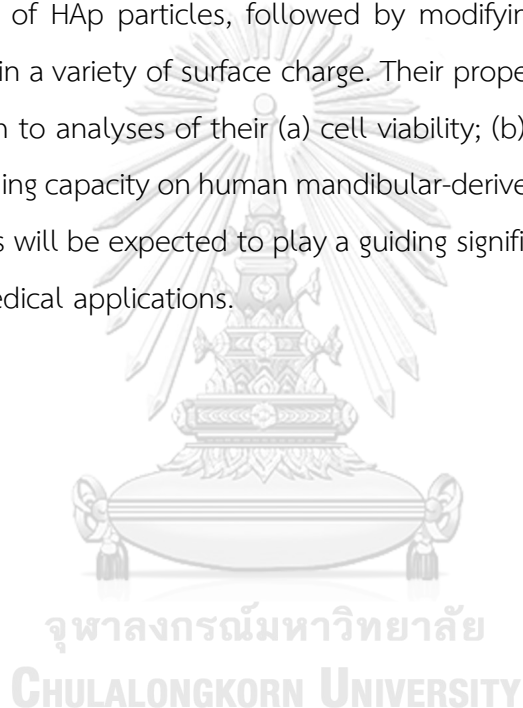
CHAPTER 3

EXPERIMENTS

In this research, the experiments are divided into three parts.

1. Synthesis of HAp nanoparticles with different sizes and shapes.

2. Surface modification of HAp nanoparticles with different surface charges.

3. Evaluation of the ability of unmodified and modified HAp nanoparticles as miRNA carrier system for human mandibular-derived osteoblast cells (hMOBs).

3.1. Materials and chemicals

All chemicals and biological reagents in this work are listed below.

Table 3.1. List of chemicals.

Chemicals	Supplier
Calcium nitrate tetrahydrate ($Ca(NO_3)_2.4H_2O$)	Sigma-Aldrich
Ammonium hydrogen phosphate (($NH_4)_2HPO_4$)	Alfa Aesar
Cetyltrimethylammonium bromide (CTAB)	Sigma-Aldrich
Ammonia solution	Merck
Ethanolamine	Merck
Polyethylene glycol (PEG6000)	Merck
Oleic acid	Sigma-Aldrich
Cyclohexane	RCI Labscan
Triton X-100	Sigma-Aldrich
n-Butanol	RCI Labscan
Ethanol	RCI Labscan
Hexane	RCI Labscan
3-aminopropyltriethoxysilane (APTES)	Sigma-Aldrich
Dichloromethane	RCI Labscan
Triethylamine	Sigma-Aldrich
2-bromoisobutyryl bromide (BIBB)	Sigma-Aldrich
2-(dimethyl amino) ethyl methacrylate (DMAEMA)	Sigma-Aldrich
Copper (I) bromide (CuBr)	Sigma-Aldrich

Chemicals	Supplier
Copper (II) bromide ($CuBr_2$)	Sigma-Aldrich
2,2′-bipyridine (Bpy)	Sigma-Aldrich
Methanol	RCI Labscan

Table 3.2. List of biological reagents.

Biological reagents	Supplier
Serum free media	GibcoTM Life Technologies
3-(4,5-dimethylthiazol-2-yl)-2,5-diphenyltetrazolium bromide (MTT)	Sigma-Aldrich
Phosphate Buffered Saline (PBS)	GibcoTM Life Technologies
Glycine	Sigma-Aldrich
Dimethyl sulfoxide (DMSO)	PanReac AppliChem
Fluorescein isothiocyanate (FITC)	Biolegend
Dulbecco's Modified Eagle's Medium (DMEM)	GibcoTM Life Technologies
miRNA	Qiagen
RNase free water	Sigma-Aldrich
Dharmafect	Qiagen
TRIzol lysis reagent	Invitrogen
ImProm-II® Reverse transcription system	Promega
FastStart Essential DNA Green Master kit	Roche Diagnostics

3.2. Synthesis of HAp nanoparticles

HAp nanoparticles with various sizes and morphologies were prepared via three methods using $Ca(NO_3)_2.4H_2O$ as a calcium precursor and $(NH_4)_2HPO_4$ as a phosphate precursor under basic condition which is described by the equation below[51]:

$$10Ca(NO_3)_2.4H_2O + 6(NH_4)_2HPO_4 + 8NH_4OH \longrightarrow Ca_{10}(PO_4)_6(OH)_2 + 20NH_4NO_3 + 22H_2O$$
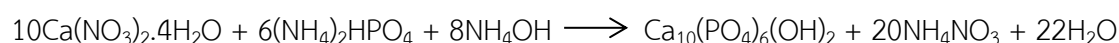
3.2.1. Wet chemical precipitation method.

This approach was modified from Wang *et al.*[52] To begin with, aqueous ammonia was added to adjust pH of 50 mL 0.3 M calcium solution and 30 mL 0.3 M phosphate solution to 10. Then, 5 wt% ethanolamine as a dispersant was added into

the calcium solution under stirred condition at 40°C. The precipitation was performed by dropwise addition of phosphate solution into the calcium mixture and further stirred for 1.5 h. Then, the reaction was placed in room temperature for 24 h. The product was separated by centrifugation and washed with ethanol and water. The obtained product was further dried overnight at 70°C.

3.2.2. Hydrothermal method.

The method proposed by Sun *et al.[53]* was followed. Firstly, 4 mL of oleic acid and 16 mL of ethanol were added to 7.5 mL of 0.25 M calcium solution containing 0.5 g PEG6000. Then, 1.125 mmol phosphate solution was dropped into the above mixture with agitation and pH of the mixture was adjusted to 10.00 using aqueous ammonia. The suspension was hydrothermally treated at 120°C for 10 h in a Teflon-lined autoclave and then water-cooled to room temperature. The precipitate was centrifuged and washed with hexane, ethanol and distilled water, respectively. Finally, the product was dried at 80°C for 24 h.

3.2.3. Reverse microemulsion under hydrothermal method.

This method was adapted from Sun *et al[54]*. Briefly, 10 mL of 0.5 M calcium solution was dropped slowly into the reverse microemulsion system of 56 mL cyclohexane, 16 mL of TX-100 and 6 mL of n-butanol. Next, 10 mL of 0.3 M phosphate solution was added into the above solution with continuous and gentle stirring. Then, the pH value was adjusted to 11.0. Finally, the obtained solution was transferred into a Teflon autoclave and heated at 160°C for 12 h. The resulted product was washed several times with ethanol and dried in an oven at 60°C for 24 h.

In order to produce the size- and shape-controllable HAp nanoparticles, the parameters of each preparation condition were investigated as summarized in Table 3.3.

Table 3.3. The parameters for preparation conditions.

Method	parameters	conditions					
Wet chemical precipitation	Ethanolamine concentration	3, 5, 10 wt%					
	pH value	8, 10, 11					
	Temperature	room temperature, 40, 60, 80°C					
Hydrothermal	pH value	7, 8, 9, 10					
	Temperature	120, 140, 160°C					
	Reaction Time	2, 5, 10 h					
Reverse microemulsion under hydrothermal	Reactant concentration	calcium solution (M)	0.17	0.25	0.50	1.00	1.50
		phosphate solution (M)	0.10	0.15	0.30	0.60	0.90
	Temperature	120, 140, 160°C					
	Reaction Time	2, 6, 12 h					

3.3. Surface modification of HAp nanoparticles.

The surface charges of HAp nanoparticles were varied by grafting with two cationic functional molecules, 3-aminopropyltriethoxysilane (APTES) and poly (2-dimethylaminoethyl methacrylate) (PDMAEMA).

3.3.1. Preparation of 3-aminopropyltriethoxysilane (APTES) coated on HAp nanoparticles (HAp-NH$_2$).

The silanization of HAp was performed according to previously reported[55] as demonstrated in Figure 3.1[56].

Figure 3.1. Reaction of functionalizing APTES on HAp nanoparticles.

0.2 g HAp was redispersed in 20 mL of 2.5 %v/v APTES solution in anhydrous toluene. The suspension was stirred for 3 h at room temperature, followed by separation in a centrifuge and washing with toluene. The obtained solid was dried at 60°C for 24 h to produce the HAp coated with terminal –NH_2 groups (HAp-NH_2).

3.3.2. Preparation of poly (2-dimethylaminoethyl methacrylate) (PDMAEMA) grafted HAp nanoparticles (HAp-PDMAEMA).

The functionalization of HAp with PDMAEMA was carried out in two steps similar to an earlier research[50] (Figure 3.2.).
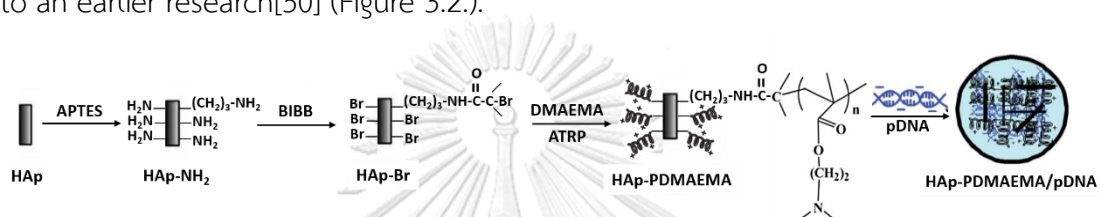
Figure 3.2. Reaction of functionalizing PDMAEMA on HAp nanoparticles.[50]

3.3.2.1. Preparation of 2-bromoisobutyryl-immobilized HAp nanoparticles (HAp-Br).

Firstly, 5 g of HAp-NH_2 obtained from Step 3.3.1. was dispersed in a mixture of dichloromethane 40 mL and triethylamine 1.5 mL by sonicating for 30 minutes. Then, the 3 mL of 2-bromoisobutyryl bromide (BIBB) in 10 mL of dichloromethane was added to the above suspension. The reaction was stirred at 0°C for 2 h and at room temperature for 24 h to obtain the HAp-Br nanoparticles. Finally, HAp-Br was washed with DI water and freeze dried overnight.

3.3.2.2. Preparation of PDMAEMA-grafted HAp nanoparticles (HAp-PDMAEMA).

Addition of 0.2 g of HAp-Br in a mixture of [3 mL of 2-(dimethyl amino) ethyl methacrylate, DMAEMA (18.7mmol)] : [$CuBr_2$] : [CuBr] : [2,2′-bipyridine, Bpy] of 100 : 0.2 : 1 : 2 in 6 ml of 4 mL of methanol and 2 mL of water and stirred at room temperature for 30 minute under the ATRP condition. The polymerization reaction was stopped by water addition and washed with deionized water to obtain HAp-PDMAEMA.

3.4. Characterization of HAp and polymer-coated HAp nanoparticles.

3.4.1. X-Ray Diffraction (XRD).

The identification of crystal phase and the degree of crystallinity were investigated by X-Ray Diffraction (XRD, D/MAX 2200 X-ray diffractometer, Rigaku, Japan) technique with Cu K$_\alpha$ incident radiation (40 kV, 30 mA). The XRD data was measured at room temperature over the 2θ range of 20–60°. The phase compositions were confirmed by comparing with the standard HAp X-Ray Diffraction pattern.

3.4.2. Fourier-Transform Infrared Spectrophotometer (FT-IR).

The functional groups were analyzed via Fourier-Transform Infrared Spectrophotometer (FT-IR, Nicolet 6700) using a KBr pellet technique. FT-IR spectra were recorded in the region of 400 cm^{-1}–4000 cm^{-1} in a transmission mode.

3.4.3. Transmission Electron Microscope (TEM).

The particle sizes and morphological features were characterized using Transmission Electron Microscope (TEM, JEOL 2100, Japan). Samples for TEM were prepared by dropping an ethanol suspension of particles on a formvar-coated copper grid and dried at room temperature. The average particle sizes were obtained using ImageJ software counting about 100 particles in several images obtained from different regions of the sample.

3.4.4. Particle size and Zeta potential measurement.

The hydrodynamic size and zeta-potential of the samples were determined using a Zetasizer (Zetasizer Nano, Malvern Instruments Ltd, UK). Samples were prepared by dispersing particles in milli-Q water with pH 7 and measured at 25°C using disposable folded capillary cells. Each value was gotten from the average of triplicate measurements.

3.5. Cell viability assay.

Cytotoxicity of HAp nanoparticles were performed on human mandibular-derived osteoblast cells (hMOBs) obtained from alveolar bone at impacted mandibular third molar of healthy patients using MTT cell viability assay.

After steam sterilization, HAp nanoparticles were dispersed in cell culture media with the concentration of 20, 50 and 100 µg/mL. Cells were cultured to 100% confluence in 96-well plates and then were treated with 100 µL of three concentrations of the nanoparticles at 24, 48 and 72 h. After treatment, media was carefully replaced with 100 µL of MTT solution and incubated in a humidified atmosphere at 37 $^\circ$C with 5% CO_2 for 30 min. Finally, the media was removed and washed with PBS. Afterward, 100 µL of the glycine solution (125 µL glycine and 900 µL DMSO) was added to dissolve the purple formazan crystal. The %cell viability was calculated compared to the control group (non-MTT treated cells defined as 100%) by measuring the absorbance at 570 nm with reference to wavelength of 690 nm using a microplate reader (SpectraMax M5, Molecular device). Each experiment was done in triplicate.

3.6. Cellular uptake efficiency.

The quantitative analysis on cellular uptake of HAp nanoparticles on human mandibular-derived osteoblast cells (hMOBs) was measured by a flow cytometry using fluorescein isothiocyanate (FITC) dye for particle representing in cells.

FITC-labeled HAp nanoparticles were performed by dispersing HAp nanoparticles in 0.2 mg/mL of FITC in ethanol for 3 h. The FITC tagged particles were centrifuged and washed with ethanol to remove excess FITC. The obtained samples were dried at 60 $^\circ$C for 24 h. After that, HAp-FITC nanoparticles were redispersed in DMEM with concentration of 20, 50 and 100 ppm and 1 mL of the sample was incubated with 100,000 hMOBs in 12 well plate. After 24 h, cells were harvested by trypsinization, washed with PBS and resuspended in 100 µl PBS for a flow cytometry analysis (FACSCaliburTM; BD Bioscience, NJ, USA). The percentage of FITC-positive cells in total population was quantified to estimate the cellular uptake of HAp nanoparticles and the non-HAp treated cells were applied as the blank control. All the tests were performed in triplicate.

3.7. miRNA loading capacity.

The miRNA loading capacity of HAp nanoparticles was investigated based on Bakan *et al.[49]*.

Complexes of miRNA/HAp nanoparticles were obtained by mixing 20, 50, 100 µg/mL HAp with a solution of 380 ng of miRNA302a in 10 µL RNase free water at room temperature under gentle shaking for 30 min. After that, the samples were centrifuged at 12,000 rpm for 10 min and miRNA quantification of supernatant was analyzed by measuring an absorbance at 260/280 nm via a Micro-Volume UV-Vis Spectrophotometer for Nucleic Acid and Protein Quantification (Thermo Scientific, Nanodrop 2000). The miRNA loading capacity of HAp was calculated compared to the 380 ng miRNA in 10 µL RNase free water without HAp as a control group by the equation of:

$$\text{miRNA loading capacity} = \frac{miRNA\ conc.of\ control - miRNA\ conc.of\ HAp}{miRNA\ conc.of\ control} \times 100$$

3.8. Statistical analysis.

All data are expressed as mean ± standard deviation of a representative three independent experiments carried out in triplicate. Statistically significant differences of means were determined via one-way ANOVA Tukey HSD at $p < 0.05$. All statistical analyses were performed using SPSS software.

CHAPTER 4

RESULTS AND DISCUSSION

This chapter describes the results and discussion based on the data collected from unmodified HAp nanoparticles prepared via three synthesis approaches and modified HAp nanoparticles with cationic surfactants. The ability of both HAp groups as miRNA delivery system were evaluated by combined analyses data include their characterization, *in vitro* cytotoxicity study, cellular uptake efficiency, and miRNA loading capacity.

4.1. Characterization of HAp nanoparticles.

4.1.1. X-Ray Diffraction (XRD).

The XRD patterns of the products synthesized via three methods under various conditions are given in Figure 4.1. Phase analysis of all samples was indexed to hexagonal structure of HAp corresponding to the standard data of HAp crystal (JCPDS no.74-0565) without the presence of secondary phases. Additionally, high crystallinity of sharp HAp peaks was observed in the samples hydrothermally treated via hydrothermal and reverse microemulsion under hydrothermal method (Figure 4.1b and c). In contrast, the effect of experimental conditions on the crystallinity based on the relative intensities of (211), (300), and (202) peaks was observed in particles obtained from wet chemical precipitation method (Figure 4.1a). The degree of crystallinity became increasing in the experiment using low ethanolamine concentration at pH over 10 under high synthesis temperature.
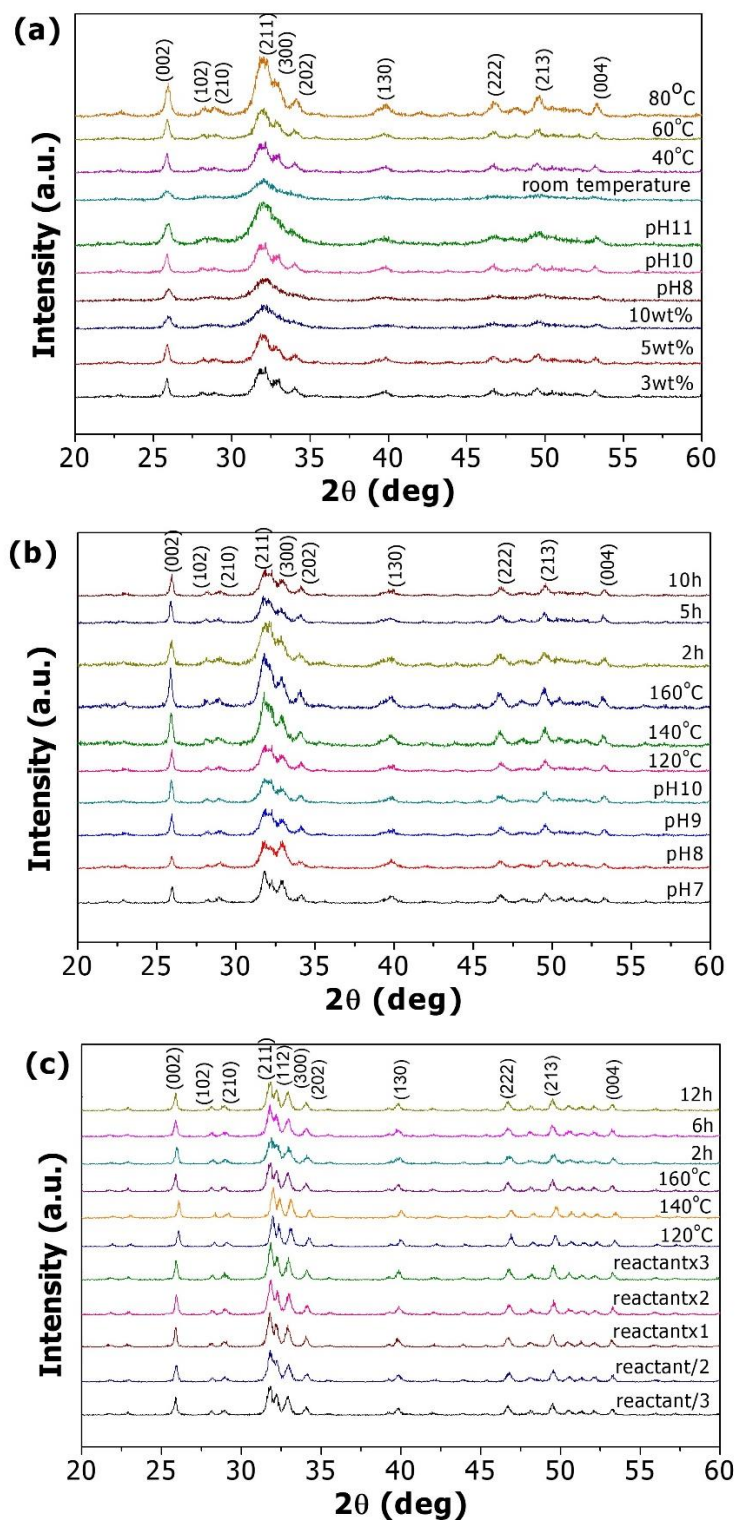
Figure 4.1. XRD patterns of HAp nanoparticles synthesized with different experimental conditions via three synthesis methods: (a) wet chemical precipitation, (b) hydrothermal and (c) reverse microemulsion under hydrothermal.

4.1.2. Fourier-Transform Infrared Spectrophotometer (FT-IR).

The FT-IR spectra of synthetic HAp series using different synthesis method were demonstrated in Figure 4.2. All particles exhibited the characteristic absorption peaks corresponding to functional groups of HAp powder. The weak and narrow peak at about 3570 cm^{-1} is assigned to the stretching and bending vibration of hydroxyl groups (OH^-). The two peaks appeared at 564 cm^{-1} and 601 cm^{-1} correspond to V_4 vibrations of the O-P-O mode, and very strong peaks occurring at 1032 cm^{-1} and 1092 cm^{-1} are associated with V_3 vibration of the P-O. In addition, the broad peak in range of 3600 to 3300 cm^{-1} presents an absorbed water in HAp structure and the peak at 1384 cm^{-1} also reveals the presence of CO_3^{2-} group due to interaction between the HAP precursor alkaline solution and atmospheric carbon dioxide[11]. Notably, the two weak peaks located at 2925 cm^{-1} and 2845 cm^{-1} are in consistent with C-H stretching vibrations of CH_3 and CH_2 groups that were found in hydrothermal powder, suggesting the presence of remaining oleic acid as a dispersant attached to the particles[53].
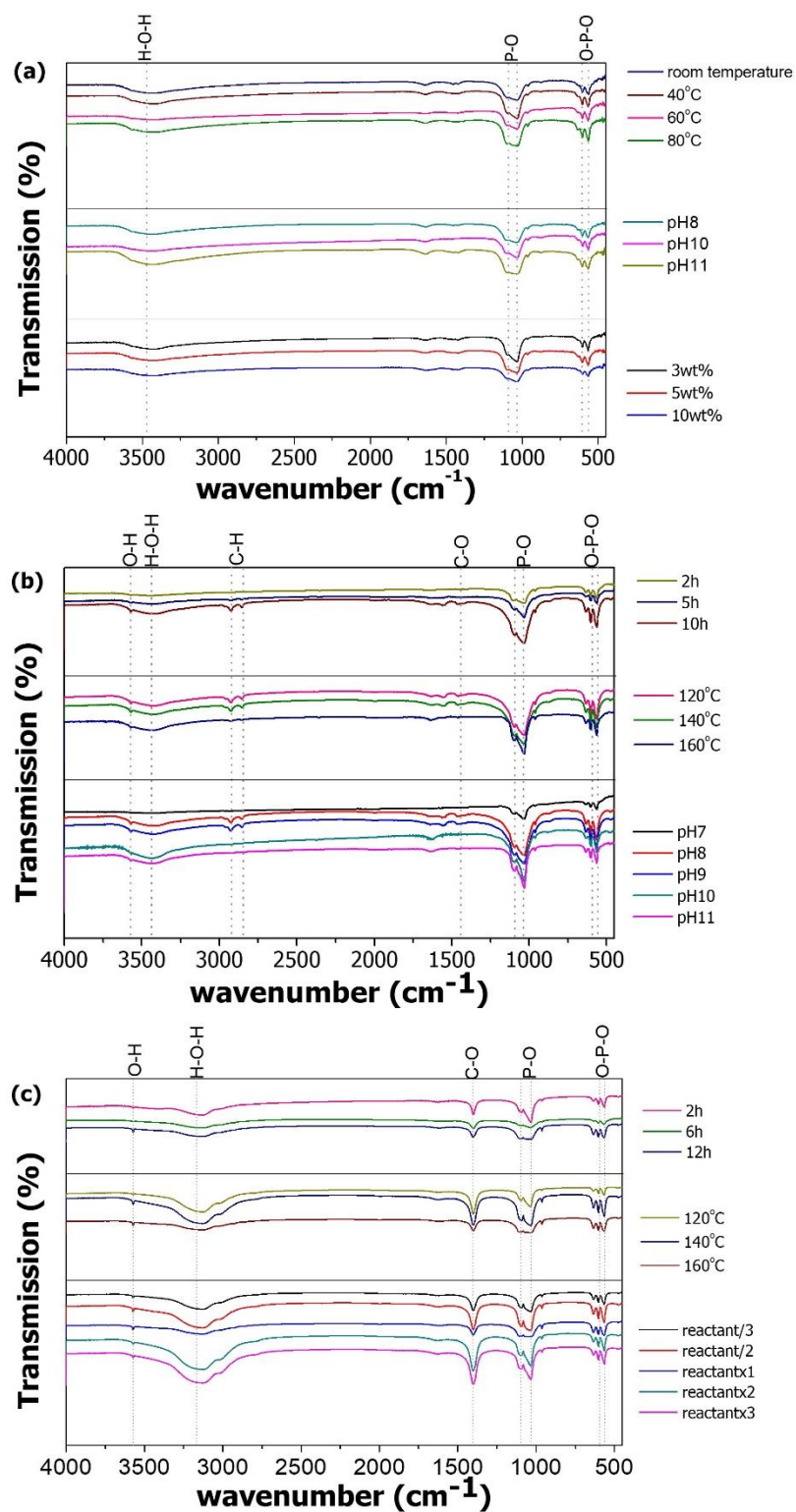
Figure 4.2. FT-IR spectra of HAp nanoparticles synthesized with different experimental conditions via three synthesis methods: (a) wet chemical precipitation, (b) hydrothermal and (c) reverse microemulsion under hydrothermal.

4.1.3. Transmission Electron Microscope (TEM).

The difference in size and morphology for prepared HAp particles obtained from different synthesis routes were illustrated in TEM micrographs as described below.

4..1.3.1. Wet chemical precipitation method.

As shown in Figure 4.3, the morphology of HAp was obviously changed from less distinct border irregular shape with 20-30 nm length and 5-10 nm width to aggregated rod-like particle with 150-200 nm length and about 20 nm width along with the decreasing of ethanolamine concentration at pH higher than 10 with rising of the reaction temperature. This finding is in consistent with the observation of higher crystallinity trend in the regular shape powder as confirmed by XRD technique.
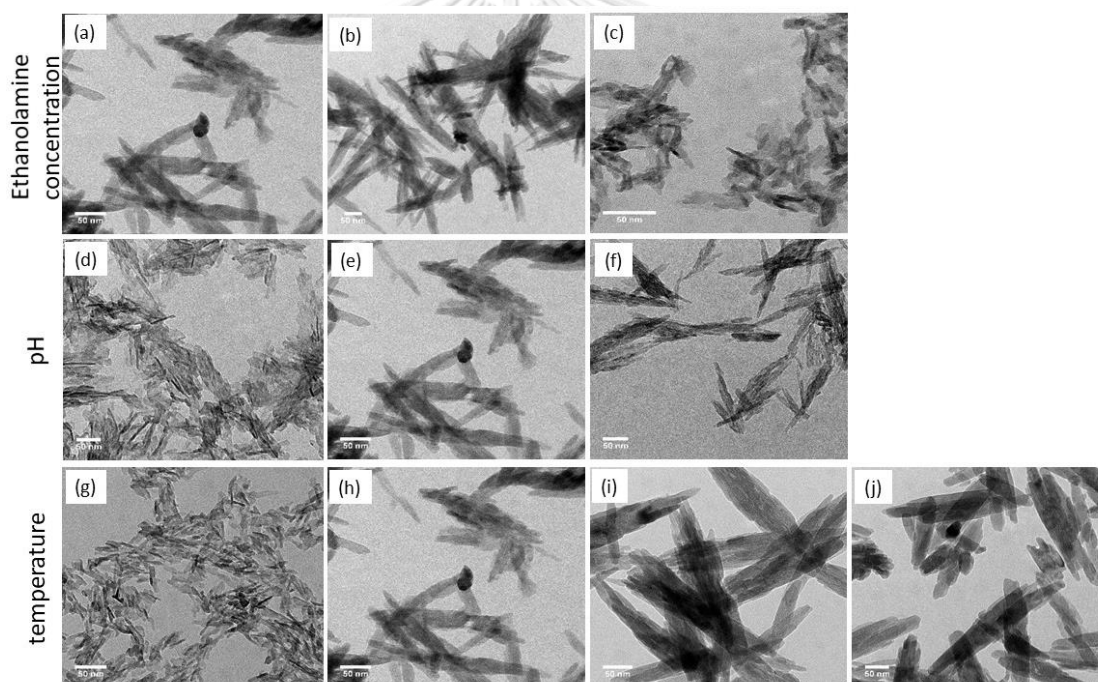
Figure 4.3. TEM images of synthesized HAp nanoparticles by wet chemical precipitation method with different synthesis conditions: (a) 3, (b) 5, (c) 10 wt% ethanolamine at pH (d) 8, (e) 10, (f) 11 under (g) room temperature, (h) 40, (i) 60, (j) 80°C. (Scale bar= 50 nm)

4.1.3.2. Hydrothermal method.

As observed in Figure 4.4, pH values, reaction temperature and time of hydrothermal method play an important role on the growth mechanism of oriented HAp crystals and result in different particle morphology. The aggregated plate-like shape with an average of 400 nm length and 100 nm width were produced using pH 7. The morphology subsequently changed to well-disperse elongated particles with size ranging from 100 to 150 nm length and about 10 nm width by altering pH value higher than 8. The good dispersibility of the particles may be resulted from the existence of surfactant covered the product as confirmed in FT-IR analysis, and the influence of pH level on particle morphology can be explained by a decrease in some crystallite facets growth rate due to the increased amount of OH⁻ ions in the solution creating surface defects in the plane of growth[57]. Furthermore, no variation of the elongated morphology is noticed through varying the reaction temperature, as opposed to the reaction time that influenced the transformation of agglomerated irregular shape with 250 nm length and 100 nm width at 2 h to thin needle-like shape with 100 nm length and about 5 nm width at 5 h and were completely grown to elongated particles after 10 h.
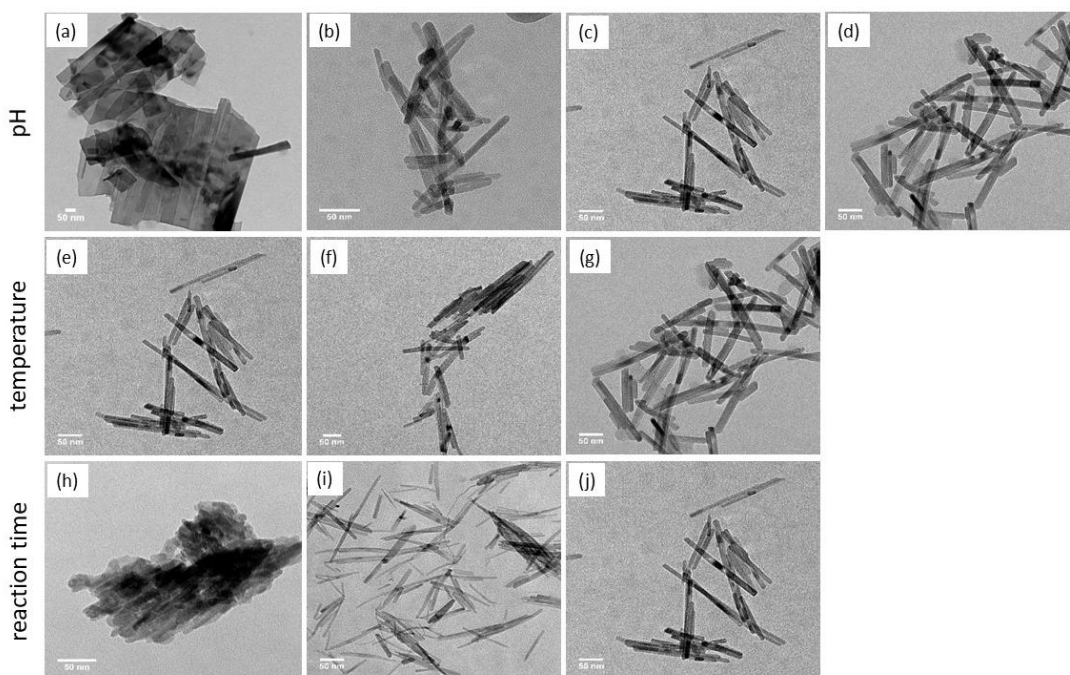
Figure 4.4. TEM images of HAp nanoparticles synthesized by hydrothermal method with different synthesis conditions: pH (a) 7, (b) 8, (c) 9, (d) 10 under (e) 120, (f) 140, (g) 160°C for (h) 2, (i) 5, (j) 10 h. (Scale bar= 50 nm)

4.1.3.3. Reverse microemulsion under hydrothermal method.

Figure 4.5 displays the TEM images of HAp with well-defined polydisperse rod-like morphology with an average length of 100 nm and width of 25-30 nm. There were no obviously change in particles shape and size with varying reactant concentration and reaction time. However, higher reaction temperature of heating at 120, 140 and 160 °C led to a slight increase in length extending from 70, 80 to 100 nm, respectively. This finding is in agreement with the report of Loo *et al.* who suggested that higher reaction temperature supplies higher amounts of driving force, resulting in the fast growth rate along c-axis of the particles[58].
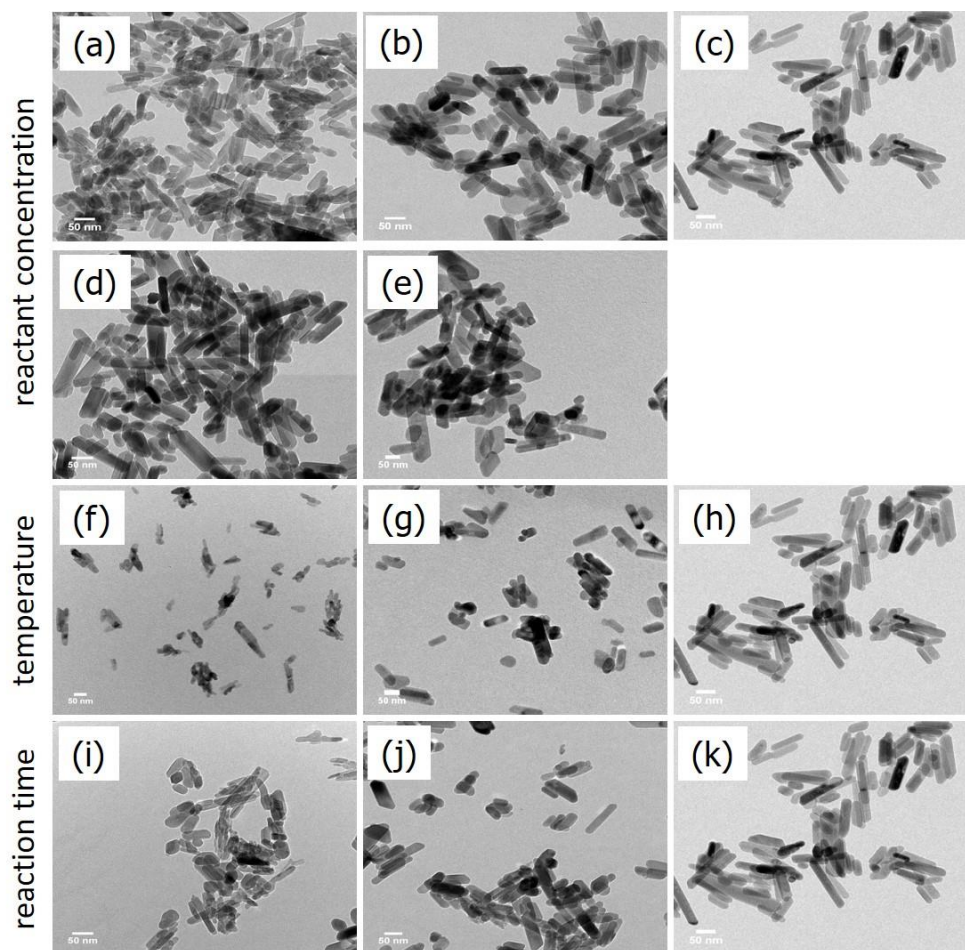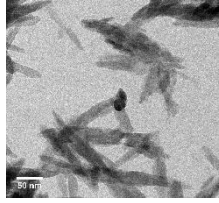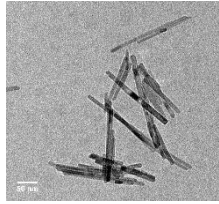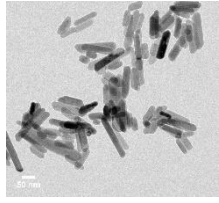
Figure 4.5. TEM images of HAp nanoparticles synthesized by reverse microemulsion under hydrothermal method with different synthesis conditions: (a) 0.17 and 0.1 , (b) 0.25 and 0.15, (c) 0.5 and 0.3, (d) 1.0 and 0.6, (e) 1.5 and 0.9 M of calcium and phosphate solution, respectively under (f) 120, (g) 140, (h) 160°C for (i) 2, (j) 6, (k) 12 h. (Scale bar= 50 nm)

Based on the above results and discussion, the characters of HAp nanoparticles with various crystallinities, sizes and morphologies provided the opportunity to investigate the relationship between HAp nanoparticle features to biological activities. Three different types of HAp nanoparticles with uniform size and morphology were chosen to assess their performance in further studies. The comparison of HAp nanoparticles properties obtained from three synthesis approaches were presented in Table 4.1.

Table 4.1. Comparison the features of three HAp types obtained from different synthesis routes.

Particle	Synthesis condition	The degree of crystallinity	Particle morphology	Particle size (nm)	TEM image
HAp1	Wet chemical precipitation: 3 wt% ethanolamine, pH 10, 40°C	High	Aggregated rod-like shape	Length: 150-200 Width: about 20	
HAp2	Hydrothermal: pH 9, 120°C, 10 h	High	Well-disperse elongated shape	Length: 100-150 Width: about 10	
HAp3	Reverse microemulsion under hydrothermal: pH 9, 160°C, 12 h	High	Well-defined polydisperse rod-like shape	Length: 100 Width: 25-30	

4.1.4. Zeta potential measurement.

The zeta potential of selected HAp suspended in milli-Q water (pH 7) were demonstrated in Figure 4.6. All particles revealed the negative value of zeta-potential of -9.97 ± 0.03, -17.43 ± 0.97 and -14.7 ± 0.79 mV for HAp1, 2 and 3, respectively. This negative charge is probably originated from -OH group in the nano-sized HAp powders[59]. The high absolute zeta potential value of HAp2 and 3 also indicated the high electrostatic stability and well-disperse of suspension in water which coincide with the TEM results. This high value may be due to the ionization of oleic acid and TX-100 as a surfactant group of HAp2 and 3 in water[60].
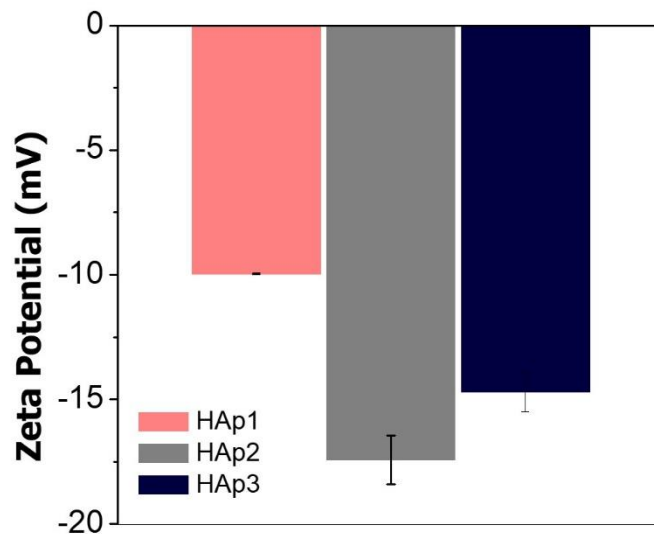
Figure 4.6. Zeta potential of HAp nanoparticles with different synthesis approaches. Data represent mean ± SD (n = 3).

4.2. *In vitro* cytotoxicity study of HAp nanoparticles.

The MTT assay was employed to evaluate the effect of different HAp size and shape on the cytotoxicity of hMOBs. As shown in Figure 4.7, the 100-150 nm length with elongated shape of HAp2 and 100 nm length with rod-like shape of HAp3 exhibited no cytotoxicity with almost 80-100 %cell viability even at the maximum concentration of 100 ppm HAp and incubation time reached to 72 h. In contrast, large particles of 150-200 nm length in rod-like shape (HAp1) was considered cytotoxicity to hMOBs with live cells count less than 80% in all concentration at every time point. This phenomenon could be explained by the report from Saunders *et al.[61]* that an increase in intracellular calcium ion from degradation process of large HAp particles may induce a mitochondrial dysfunction and possibly lead to bone cell apoptosis. This observation indicated that HAp nanoparticle size played an important role in cell toxicity. Based on this study, the biocompatibility of 100-150 nm length with elongated shape of HAp2 and 100 nm length with rod-like shape of HAp3 were selected for subsequent experiments.
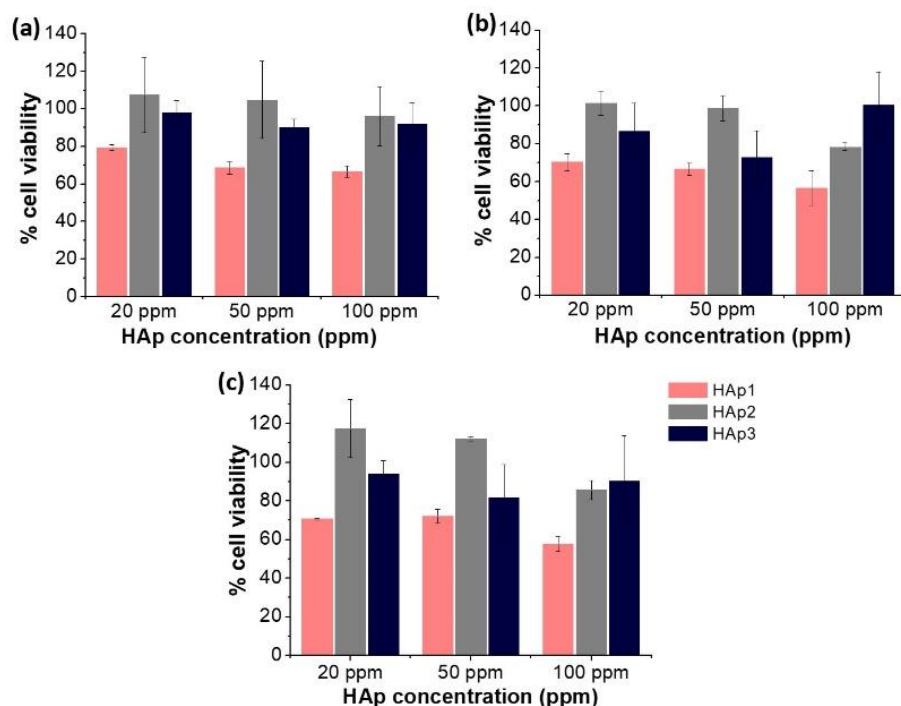
Figure 4.7. In vitro cytotoxicity of 20, 50, 100 ppm HAp nanoparticles with three synthesis methods on hMOBs after: (a) 24 h, (b) 48 h, (c) 72 h. Data represent mean ± SD (n = 3).

4.3. Cellular uptake efficiency of HAp nanoparticles.

The flow cytometry was performed to determine whether shape of two biocompatible HAp types as HAp2 and 3 can modulate the uptake of nanoparticles into hMOBs. As can be seen in Figure 4.8, the HAp2 with elongated shape had around 75-90% relative cellular uptake which was obviously two to three times higher than HAp3 with rod-like shape and no significant change was observed among the three concentration. In contrast, the number of internalized particles of HAp3 slightly increased with increasing concentration of the particles. This finding provides an additional information that the cellular uptake efficiency is strongly dependent on the particle morphology and elongated HAp2 wes the shape with the most efficient cellular uptake.
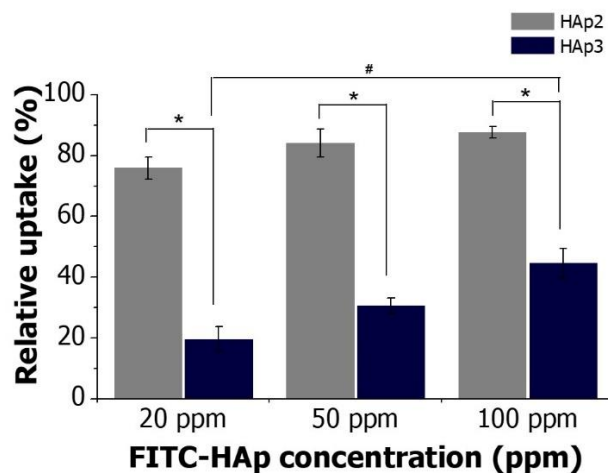
*Figure 4.8. The cellular uptake of 20, 50, 100 ppm FITC tagged HAp nanoparticles with two morphologies into hMOBs were detected by flow cytometry. *, significant difference versus two HAp groups (p < 0.05) and #p < 0.05 versus different HAp concentration.*

4.4. miRNA loading capacity of HAp nanoparticles.

The quantification of miRNA loading on two HAp nanoparticles with different morphology was also studied. The results in Figure 4.9 illustrated that miRNA binding capacity had a strong correlation with the particle morphology and concentration. The rod-like HAp3 had higher % loading efficiency compared to the elongated HAp2; however, the value was apparently less than 80% in all concentration of two HAp types. Additionally, the increasing of both particle concentrations could promote the miRNA loading ability, and the highest value was achieved at 50 ppm HAp2 and HAp3 which was at 45.29 and 70.21%, respectively. This observation could be a result of the affinity of anionic nucleic acids and calcium ions in HAp nanoparticles.[49] Therefore, higher zeta potential due to more positive calcium ion of HAp3 provided better binding behavior for negative miRNA in comparison to HAp2. Afterward, this affinity was significantly decreased with an increase in the particle concentration to 100 ppm maybe due to high aggregation of the particles at high concentration reduced the miRNA binding site. The results indicated that the improvement of miRNA loading capacity of both HAp2 and HAp3 is still required for the successful development of high-performance miRNA delivery system.
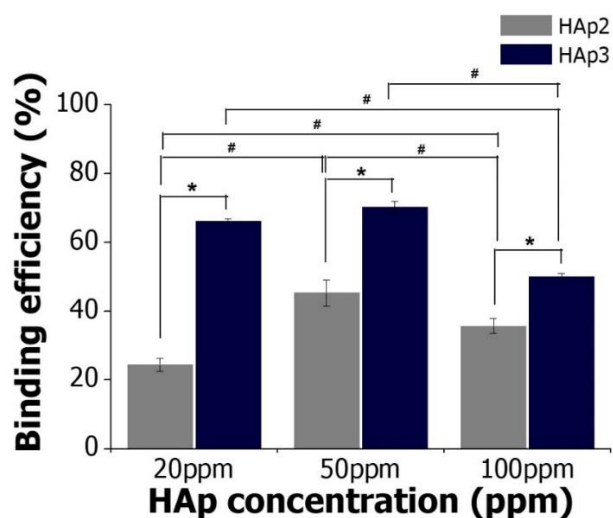
*Figure 4.9. The miRNA302a loading capacity of 20, 50, 100 ppm HAp nanoparticles with two morphologies. *, significant difference versus two HAp groups (p < 0.05) and #p < 0.05 versus different HAp concentrations.*

From overall results, the effect of size and shape of HAp on biological activity was explained. Elongated HAp2 with 100 nm length was chosen as the optimal particle with low cytotoxicity and high cellular uptake; on the other hand, it still lacks of miRNA loading capacity. Considering the gene delivery system, the surface charge has been reported as a crucial parameter of the particles for cellular transfection and interaction with miRNA molecules[62]. Consequently, the particle surface charge was further investigated in order to clarify the involvement of surface charge on the ability as miRNA delivery system by modified the HAp2 with two positive charge surfactants of two different structures, APTES and PDMAEMA.

4.5. Characterization of modified HAp nanoparticles.

4.5.1. X-Ray Diffraction (XRD).

The XRD analysis was performed to verify that two surface modification approaches for attaching HAp nanoparticles did not alter the intrinsic characteristic of HAp. As shown in Figure 4.10, no visible impact of polymer grafting and silane coupling onto HAp was observed on diffraction peaks pattern compared to unmodified HAp.

Therefore, it can be inferred that the HAp crystal structure was not destroyed during the modification process.
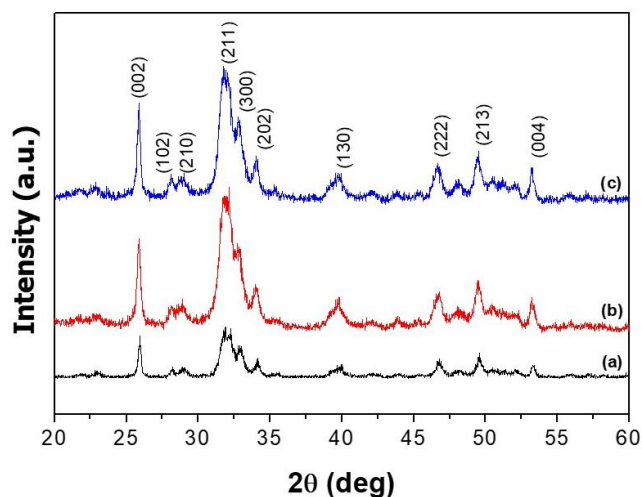
Figure 4.10. XRD patterns of (a) unmodified and modified HAp2 nanoparticles with two surfactants: (b) APTES, (c) PDMAEMA.

4.5.2. Fourier-Transform Infrared Spectrophotometer (FT-IR).

The FT-IR spectroscopy was employed to identify the functional groups of two cationic species grafted on HAp surface. As can be seen in Figure 4.11, both polymers revealed the characteristic bands related to functional groups of bare HAp. Interestingly, a new absorption peak at 1738 cm^{-1} could be observed in HAp-PDMAEMA particles, which ascribed to the stretching vibration of ester carbonyl group in the PDMAEMA[63]. This result proved that the PDMAEMA has been successfully introduced on the surface of HAp nanoparticles. In contrast, N-H stretching of amine in APTES coated HAp at the region 3400-3300 cm^{-1} cannot be verified due to the interference of broad peak of absorbed water. Therefore, the successful functionalization of APTES on HAp required further investigation.
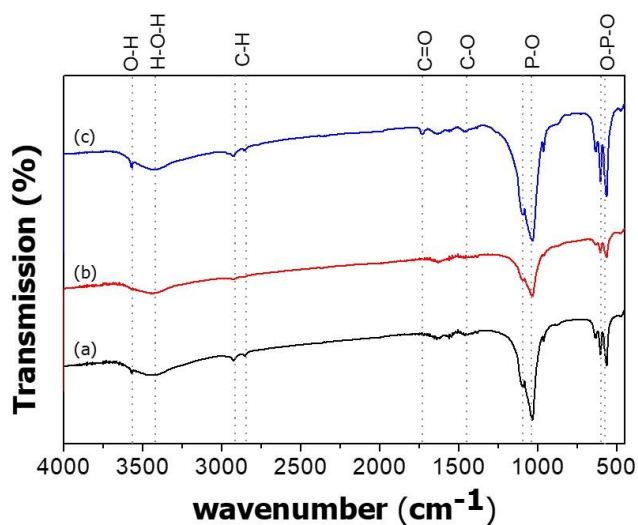
Figure 4.11. FT-IR spectra of (a) unmodified and modified HAp2 nanoparticles with two cationic species: (b) APTES, (c) PDMAEMA.

4.5.3. Transmission Electron Microscope (TEM).

The particle size and shape of the HAp nanoparticles after being grafted with two cationic surfactants were illustrated in Figure 4.12. The result demonstrated that no significant change in morphology was observed in all modified HAp nanoparticles. Functionalization with APTES had similar particle sizes to the unmodified one with 100-150 nm length and about 10 nm width in elongated shape, whereas the HAp particle size became larger with about 100-150 nm length and slightly increased in width to 15-20 nm after PDMAEMA integration.
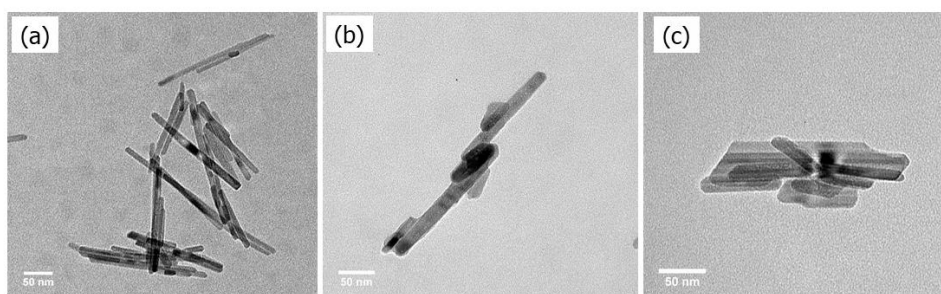
Figure 4.12. TEM images of (a) unmodified and modified HAp2 nanoparticles with two cationic species: (b) APTES, (c) PDMAEMA. (Scale bar= 50 nm)

4.5.4. Particle size and Zeta potential measurement.

The hydrodynamic size and zeta potential of the HAp nanoparticles after grafted with two cationic species were displayed in Figure 4.13. The hydrodynamic size of bare HAp was 172.8 ± 11.1 nm whereas the enhancement of the size to 260.2 ± 63.1 and 391.4 ± 11.4 nm was arisen from the coating of APTES and PDMAEMA polymers, which is in agreement with the expected trend. The layer of hydration around HAp in aqueous solution and agglomeration of the particles with high PDI values (0.5-0.8) in Zetasizer measurements led to bigger particle size than the diameter shown in TEM measurements[64]. Additionally, the surface charge of the polymer functionalized HAp became positive with zeta potential value reached 7.79 ± 0.28 and 3.29 ± 0.81 mV in HAp-APTES and HAp-PDMAEMA, respectively. This positive charge is derived from the protonation of amine of two surfactants (pKa of APTES and PDMAEMA is around 8.5 and 7.5, respectively) to cationic aminated ($-NH_3^+$) functional groups in milli-Q water with pH 7.[65] The increase of hydrodynamic size and surface charge conversion also supported that HAp nanoparticles were successfully functionalized with the two surfactants. Moreover, the Derjaguin-Landau-Verwey and Overbeek (DLVO) theory[66] stated that the high stable and less coagulation of the suspension are achieved when the electrical double layer repulsive (V_R) force related to the surface charge is higher than the van der Waals attractive force (V_A), therefore, HAp-PDMAEMA with low zeta potential value could show the aggregation of the large particles, which was observed from TEM result.
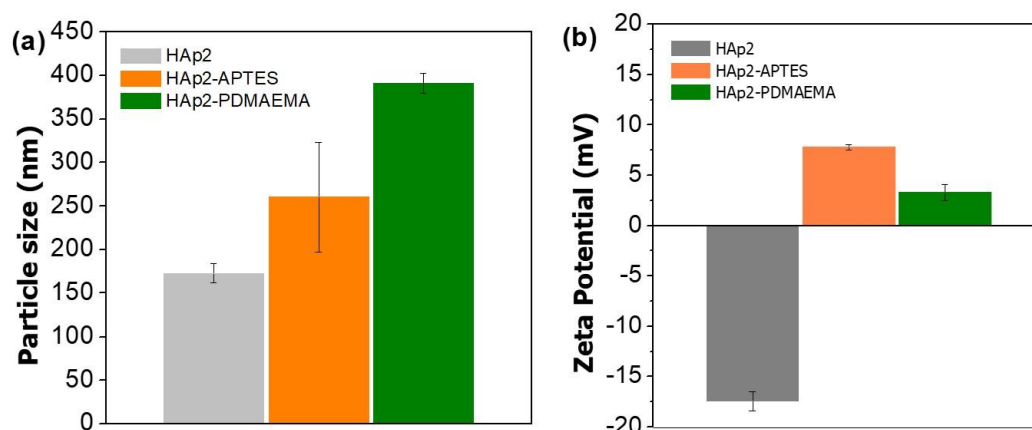
Figure 4.13. (a) Particle size and (b) Zeta potential of unmodified and modified HAp2 nanoparticles with two cationic surfactants. The error bars are standard deviations, n = 3.

4.6. *In vitro* cytotoxicity study of modified HAp nanoparticles.

The cytotoxicity of coated HAp nanoparticles on hMOBs was evaluated by MTT assay. As shown in Figure 4.14, the %cell viability was nearly 80% when treated with HAp-APTES at each concentration and even after 72 h incubation as comparable to unmodified HAp. In contrast, the cytotoxicity of PDMAEMA attachment was elevated in a linear relationship with the particle concentration. The HAp-PDMAEMA exhibited a 20% more toxic effect when incubated with a concentration of higher than 50 ppm. This may be because an aggregation and subsequent precipitation of HAp-PDMAEMA at high concentrations could mechanically damage the cells, which ultimately result in cell cytotoxicity[45]. Based on this result, HAp nanoparticles could be a safe biomaterial when modified with APTES and PDMAEMA at the maximum safety concentration of 20 ppm.
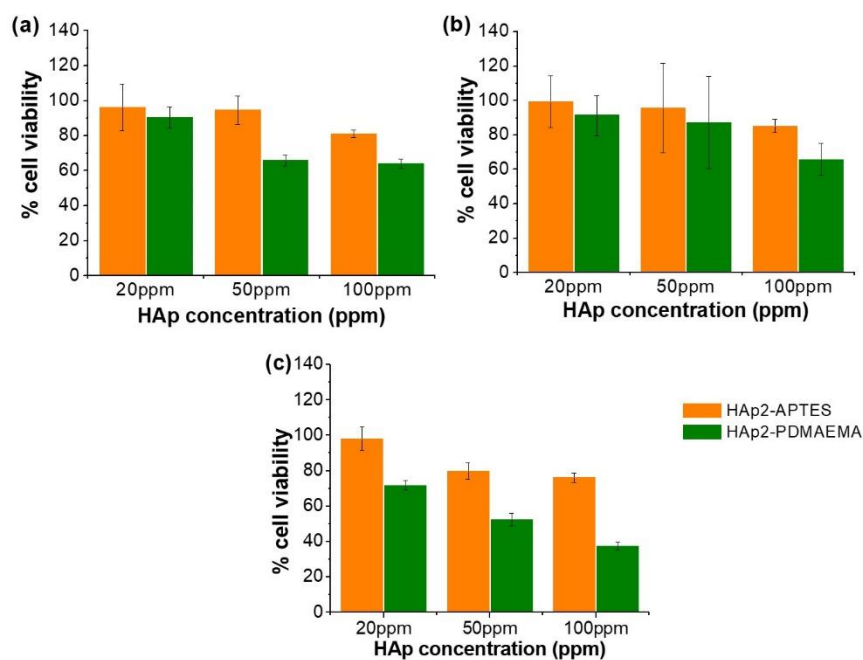
Figure 4.14. In vitro cytotoxicity of 20, 50, 100 ppm surface grafted HAp2 nanoparticles with two cationic surfactants on hMOBs after: (a) 24 h, (b) 48 h, (c) 72 h. Data represent mean ± SD (n = 3).

4.7. Cellular uptake efficiency of modified HAp nanoparticles.

To determine whether the two positive surfactants grafted on HAp nanoparticles can improve their transfection efficiency, the amount of modified HAp uptake into hMOBs was presented in Figure 4.15. It was worth noticing that modification with APTES at concentration of higher than 50 ppm and PDMAEMA at every concentration revealed a greater cellular uptake (>80%) in comparison with the unmodified HAp nanoparticles as illustrated in Figure 4.8. The intracellular uptake of HAP-APTES was obviously increased with increasing of particle concentration while no significant difference was observed in HAp-PDMAEMA. This finding is in agreement with Hu *et al[67].* who reported that positive surface charge provides a stronger electrostatic interaction with the slight negative charge of cell membrane. Thus, the presence of two cationic species on HAp nanoparticles can enhance the cellular uptake efficiency of the particles to above 80% compared to the bare ones.
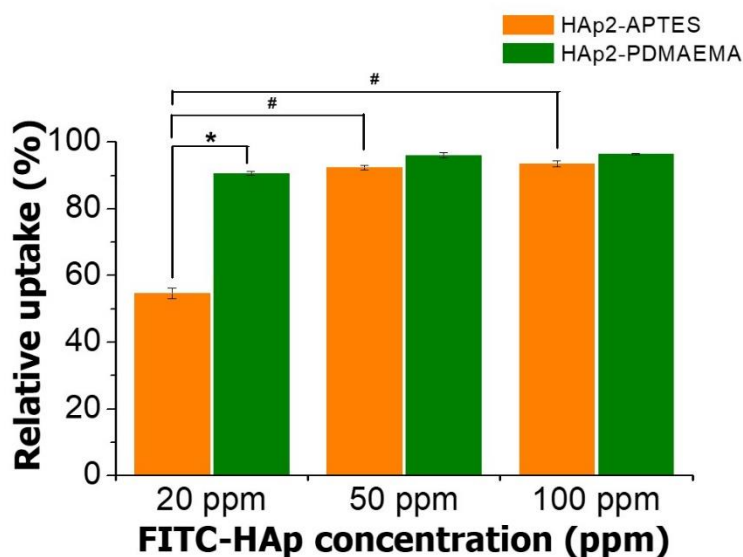
Figure 4.15. The cellular uptake of 20, 50, 100 ppm FITC tagged surface grafted HAp2 nanoparticles with two cationic surfactants into hMOBs were detected by flow cytometry. *, significant difference versus three HAp groups (p < 0.05) and ${}^{\#}p < 0.05$ versus different HAp concentrations.

4.8. miRNA loading capacity of modified HAp nanoparticles.

Beside the cellular uptake, miRNA loading capacity of HAp attached with two positive polymers is also essential to be discussed. As seen in Figure 4.16, the miRNA condensation efficiency of all HAp modified with APTES was significantly higher than the ones with PDMAEMA and unmodified HAp with the highest value of 45.29. This observation may be resulted from an increase in electrostatic interaction between positive surface charge of polymer and negatively charged miRNA. In contrast, the lower miRNA loading ability, which is found in modification PDMAEMA, could be due to a decrease in surface area of larger particle size, which is against with miRNA binding. Consequently, the attached HAp nanoparticles with APTES were the most favorable for miRNA conjugation.
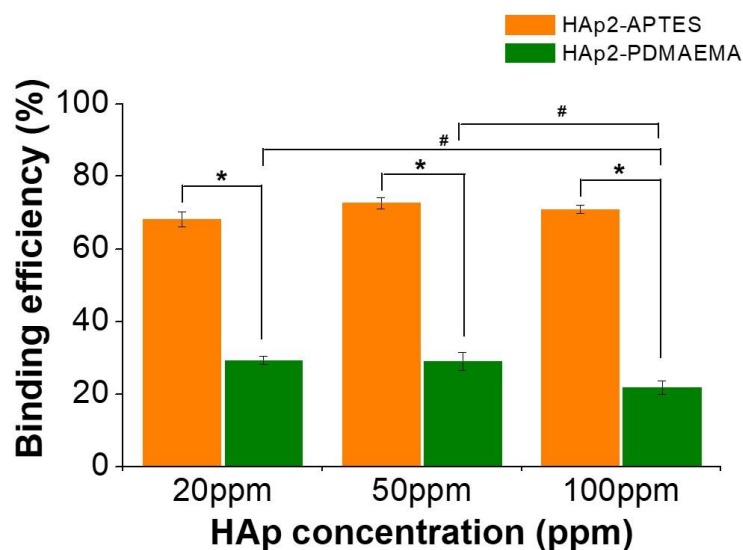
*Figure 4.16. The miRNA302a loading capacity of 20, 50, 100 ppm surface grafted HAp2 nanoparticles with two cationic surfactants. *, significant difference versus three HAp groups (p < 0.05) and #p < 0.05 versus different HAp concentrations.*

The above results revealed that the surface charge also played an importance role in cytotoxicity, intracellular uptake efficiency and miRNA condensing capacity. The highest of those all ability with low cytotoxicity was achieved after functionalized HAp with APTES; therefore, HAp-APTES could be a safe carrier for high-performance miRNA delivery system.

CHAPTER 5

CONCLUSION

In summary, this research proposes a comparative study between different particle sizes, morphologies and surface charges of HAp nanoparticles on their biological properties as miRNA delivery system for biomedical applications, especially for bone and teeth.

The rod-like HAp nanoparticles with different sizes were successfully synthesized via wet chemical precipitation and reverse microemulsion under hydrothermal approaches. The precipitation method using ethanolamine as a dispersant provided a larger aggregated HAp nanoparticle with 150-200 nm in length and about 20 nm in width; whereas, the smaller ones with well-dispersed particles of 100 nm in length and 25-30 nm in width were obtained from microemulsion method using TX-100 as a dispersant and n-butanol as a cosurfactant in cyclohexane/water system. The morphology dependent biological behaviors were also assessed from the elongated shaped HAp nanoparticle with length of 100-150 nm and width of about 10 nm synthesized by hydrothermal method using oleic acid and PEG as dispersant. The influence of particle size and shape of HAp nanoparticles on their cytotoxicity, cellular uptake ability and miRNA loading capacity were investigated on human mandibular-derived osteoblast cells (hMOBs). The cytotoxicity based on MTT assay results demonstrated that the smaller HAp nanoparticles with the size ranging from 100-150 nm of with both rod-like and elongated morphologies exhibited better biocompatibility on hMOBs compared to the one with larger size in range of 150-200 nm. Consequently, size-dependent effect of HAp particles on bone related cells was confirmed.

The biocompatible HAp particles with different morphologies of rod and elongated shape were examined for cellular uptake and miRNA binding capacities. The morphology-dependent effect of HAp particle was also illustrated in both experiments. The elongated morphology has significant higher in cellular uptake ability of around 75-90% relative cellular uptake compared to rod-like morphology even incubation at lowest concentration of 20 ppm. In contrast, the rod-like morphology has more miRNA loading efficiency than the elongated particle, and the highest value of 70.21% was

observed when miRNA incorporated with HAp nanoparticle at 50 ppm. However, the low quantity (<80%) of miRNA loading capacity of both HAp is remain the major limitation for using HAp nanoparticles as miRNA delivery agent.

To enhance the miRNA affinity, HAp with elongated morphology was chosen for elucidating the role of surface charge of the particles on their biological properties as above experiments by modified HAp particles with two cationic functional molecules: 3-aminopropyltriethoxysilane (APTES) and poly (2-dimethylaminoethyl methacrylate) (PDMAEMA). The zeta potential represented the alteration of surface charge after modification from -17.43 ± 0.97 to 7.79 ± 0.28 and 3.29 ± 0.81 mV in HAp-APTES and HAp-PDMAEMA, respectively. The cell viability results indicated that HAp-PDMAEMA has high toxicity on hMOBs after treated with concentration above 50 ppm, while, the HAp-APTES was considered as a biocompatible material with high cell viability at all concentration and incubation time reaching 72 h. Furthermore, no significant different of cellular uptake efficiency was found between both functionalized HAp particles; on the other hand, the presence of APTES on the particle revealed the significant higher ability to encapsulate miRNA compared to PDMAEMA.

These findings suggest that the elongated HAp nanoparticle with length of 100-150 nm and width of 10 nm functionalized with APTES can be considered as a potential miRNA delivery system to osteoblast cells for used in biomedical applications, particularly bone regeneration. However, the development of this miRNA based therapeutic system is still in initial phases, more investigation on biological activities of the HAp-APTES nanoparticle are needed to verify the performance of the particle as miRNA delivery carrier for bone regeneration before being widely used in clinical applications.

REFERENCES

1. Stevens, M.M., *Biomaterials for bone tissue engineering.* Materials Today, 2008. **11**(5): p. 18-25.

2. Catros, S., et al., *Physico-chemical and biological properties of a nano-hydroxyapatite powder synthesized at room temperature.* IRBM, 2010. **31**(4): p. 226-233.

3. Misch, C.E. and F. Dietsh, *Bone-grafting materials in implant dentistry.* Implant Dent, 1993. **2**(3): p. 158-67.

4. Sheikh, Z., et al., *Biodegradable Materials for Bone Repair and Tissue Engineering Applications.* Materials (Basel), 2015. **8**(9): p. 5744-5794.

5. Goudouri, O.-M., E. Kontonasaki, and A.R. Boccaccini, *Layered scaffolds for periodontal regeneration*, in *Biomaterials for Oral and Dental Tissue Engineering*. 2017. p. 279-295.

6. Markovic, S., et al., *Synthetical bone-like and biological hydroxyapatites: a comparative study of crystal structure and morphology.* Biomed Mater, 2011. **6**(4): p. 045005.

7. Hwang, H.W. and J.T. Mendell, *MicroRNAs in cell proliferation, cell death, and tumorigenesis.* Br J Cancer, 2006. **94**(6): p. 776-80.

8. Mencia Castano, I., et al., *A novel collagen-nanohydroxyapatite microRNA-activated scaffold for tissue engineering applications capable of efficient delivery of both miR-mimics and antagomiRs to human mesenchymal stem cells.* J Control Release, 2015. **200**: p. 42-51.

9. Lin, K. and J. Chang, *Structure and properties of hydroxyapatite for biomedical applications*, in *Hydroxyapatite (Hap) for Biomedical Applications*. 2015. p. 3-19.

10. Fihri, A., et al., *Hydroxyapatite: A review of syntheses, structure and applications in heterogeneous catalysis.* Coordination Chemistry Reviews, 2017. **347**: p. 48-76.

11. Poinern, G.J., et al., *Thermal and ultrasonic influence in the formation of nanometer scale hydroxyapatite bio-ceramic.* Int J Nanomedicine, 2011. **6**: p. 2083-95.

12. Bakan, F., *Gene Delivery by Hydroxyapatite and Calcium Phosphate Nanoparticles: A Review of Novel and Recent Applications*. 2018.

13. Noori-Daloii, M.R. and A. Nejatizadeh. *MicroRNAs in Disease and Health : Diagnostic and Therapeutic Potentials.* 2018.

14. Felekkis, K., et al., *microRNAs: a newly described class of encoded molecules that play a role in health and disease.* Hippokratia, 2010. **14**(4): p. 236-40.

15. Sriram, M., et al., *Biomaterials mediated microRNA delivery for bone tissue engineering.* Int J Biol Macromol, 2015. **74**: p. 404-12.

16. Tanase, C.P., I. Ogrezeanu, and C. Badiu, *MicroRNAs*, in *Molecular Pathology of Pituitary Adenomas*. 2012. p. 91-96.

17. Rupaimoole, R., et al., *MicroRNA therapeutics: principles, expectations, and challenges.* Chin J Cancer, 2011. **30**(6): p. 368-70.

18. Rodriguez-Lugo, V., et al., *Wet chemical synthesis of nanocrystalline hydroxyapatite flakes: effect of pH and sintering temperature on structural and morphological properties.* R Soc Open Sci, 2018. **5**(8): p. 180962.

19. Sadat-Shojai, M., et al., *Synthesis methods for nanosized hydroxyapatite with diverse structures.* Acta Biomater, 2013. **9**(8): p. 7591-621.

20. Bayazit, V., M. Bayazit, and E. Bayazit, *Evaluation of bioceramic materials in biology and medicine*. Vol. 7. 2010. 211-222.

21. Sadat-Shojai, M., M. Atai, and A. Nodehi, *Design of Experiments (DOE) for the Optimization of Hydrothermal Synthesis of Hydroxyapatite Nanoparticles*. Vol. 22. 2011. 571-582.

22. Sadat-Shojai, M., et al., *Hydroxyapatite nanorods as novel fillers for improving the properties of dental adhesives: Synthesis and application.* Dent Mater, 2010. **26**(5): p. 471-82.

23. Gshalaev, V.S. and A.C. Demirchan, *Hydroxyapatite: Synthesis, properties and applications*. 2013. 1-477.

24.   Lim, G.K., et al., *Processing of hydroxyapatite via microemulsion and emulsion routes.* Biomaterials, 1997. **18**(21): p. 1433-1439.

25.   Zhou, W.Y., et al., *Synthesis of carbonated hydroxyapatite nanospheres through nanoemulsion.* J Mater Sci Mater Med, 2008. **19**(1): p. 103-10.

26.   Okada, M. and T. Furuzono, *Hydroxylapatite nanoparticles: fabrication methods and medical applications.* Sci Technol Adv Mater, 2012. **13**(6): p. 064103.

27.   Lai, C., Y.J. Wang, and K. Wei, *Nucleation kinetics of calcium phosphate nanoparticles in reverse micelle solution.* Colloids and Surfaces A: Physicochemical and Engineering Aspects, 2008. **315**(1-3): p. 268-274.

28.   Siddiqui, J.A. and N.C. Partridge, *Physiological Bone Remodeling: Systemic Regulation and Growth Factor Involvement.* Physiology (Bethesda), 2016. **31**(3): p. 233-45.

29.   Hadjidakis, D.J. and Androulakis, II, *Bone remodeling.* Ann N Y Acad Sci, 2006. **1092**: p. 385-96.

30.   Saftig, P., et al., *Impaired osteoclastic bone resorption leads to osteopetrosis in cathepsin-K-deficient mice.* Proc Natl Acad Sci U S A, 1998. **95**(23): p. 13453-8.

31.   Manolagas, S.C., *Birth and death of bone cells: basic regulatory mechanisms and implications for the pathogenesis and treatment of osteoporosis.* Endocr Rev, 2000. **21**(2): p. 115-37.

32.   Jilka, R.L., et al., *Osteoblast programmed cell death (apoptosis): modulation by growth factors and cytokines.* J Bone Miner Res, 1998. **13**(5): p. 793-802.

33.   Raisz, L.G., *Physiology and pathophysiology of bone remodeling.* Clin Chem, 1999. **45**(8 Pt 2): p. 1353-8.

34.   Crockett, J.C., et al., *Bone remodelling at a glance.* J Cell Sci, 2011. **124**(Pt 7): p. 991-8.

35.   Owen, R. and G.C. Reilly, *In vitro Models of Bone Remodelling and Associated Disorders.* Front Bioeng Biotechnol, 2018. **6**: p. 134.

36.   Xing, L. and B.F. Boyce, *Regulation of apoptosis in osteoclasts and osteoblastic cells.* Biochem Biophys Res Commun, 2005. **328**(3): p. 709-20.

37.   Kenkre, J.S. and J. Bassett, *The bone remodelling cycle.* Ann Clin Biochem, 2018. **55**(3): p. 308-327.

38. Bernstein, J. *Describe the process of bone remodeling*. 2011 Jan 11, 2014; Available from: https://www.orthopaedicsone.com/x/MAJCB.

39. Sozen, T., L. Ozisik, and N.C. Basaran, *An overview and management of osteoporosis.* Eur J Rheumatol, 2017. **4**(1): p. 46-56.

40. Uskokovic, V., et al., *Effect of calcium phosphate particle shape and size on their antibacterial and osteogenic activity in the delivery of antibiotics in vitro.* ACS Appl Mater Interfaces, 2013. **5**(7): p. 2422-31.

41. Hoai, T.T., et al., *Hydrothermal Synthesis of Hydroxyapatite Nanorods for Rapid Formation of Bone-Like Mineralization.* Journal of Electronic Materials, 2017. **46**(8): p. 5064-5072.

42. Lin, Z., et al., *MicroRNA-92a-1-5p influences osteogenic differentiation of MC3T3-E1 cells by regulating beta-catenin.* J Bone Miner Metab, 2019. **37**(2): p. 264-272.

43. Yang, C., et al., *miRNA-21 promotes osteogenesis via the PTEN/PI3K/Akt/HIF-1alpha pathway and enhances bone regeneration in critical size defects.* Stem Cell Res Ther, 2019. **10**(1): p. 65.

44. Mencia Castano, I., et al., *Next generation bone tissue engineering: non-viral miR-133a inhibition using collagen-nanohydroxyapatite scaffolds rapidly enhances osteogenesis.* Sci Rep, 2016. **6**: p. 27941.

45. Yang, X., et al., *In Vitro Uptake of Hydroxyapatite Nanoparticles and Their Effect on Osteogenic Differentiation of Human Mesenchymal Stem Cells.* Stem Cells Int, 2018. **2018**: p. 2036176.

46. Shi, Z., et al., *Size effect of hydroxyapatite nanoparticles on proliferation and apoptosis of osteoblast-like cells.* Acta Biomater, 2009. **5**(1): p. 338-45.

47. Huang, Q., et al., *Morphologically Controlled Synthesis of Hydroxyapatite and Its Bioactivity on Osteoblast Cells.* Journal of Nanoscience and Nanotechnology, 2016. **16**(7): p. 6978-6985.

48. Chen, L., et al., *The role of surface charge on the uptake and biocompatibility of hydroxyapatite nanoparticles with osteoblast cells.* Nanotechnology, 2011. **22**(10): p. 105708-105708.

49. Bakan, F., et al., *Synthesis and characterization of amino acid-functionalized calcium phosphate nanoparticles for siRNA delivery.* Colloids Surf B Biointerfaces, 2017. **158**: p. 175-181.

50. Cai, Q., et al., *Well-defined hydroxyapatite–polycation nanohybrids via surface-initiated atom transfer radical polymerization for biomedical applications*. Vol. 22. 2012. 9358-9367.

51. Kaiying, L. and Q. Jianhua, *Droplet-fused microreactors for room temperature synthesis of nanoscale needle-like hydroxyapatite.* Nanotechnology, 2013. **24**(12): p. 125602.

52. Wang, P., et al., *Effects of synthesis conditions on the morphology of hydroxyapatite nanoparticles produced by wet chemical process.* Powder Technology, 2010. **203**(2): p. 315-321.

53. Sun, J., et al., *Monodisperse selenium-substituted hydroxyapatite: Controllable synthesis and biocompatibility.* Mater Sci Eng C Mater Biol Appl, 2017. **73**: p. 596-602.

54. Sun, Y., et al., *Reverse microemulsion-directed synthesis of hydroxyapatite nanoparticles under hydrothermal conditions.* Journal of Physics and Chemistry of Solids, 2007. **68**(3): p. 373-377.

55. Russo, L., et al., *Carbonate hydroxyapatite functionalization: a comparative study towards (bio)molecules fixation.* Interface Focus, 2014. **4**(1): p. 20130040.

56. Balasundaram, G., M. Sato, and T.J. Webster, *Using hydroxyapatite nanoparticles and decreased crystallinity to promote osteoblast adhesion similar to functionalizing with RGD.* Biomaterials, 2006. **27**(14): p. 2798-805.

57. Bilton, M., S. Milne, and A. P. Brown, *Comparison of Hydrothermal and Sol-Gel Synthesis of Nano-Particulate Hydroxyapatite by Characterisation at the Bulk and Particle Level*. Vol. 2. 2012. 1-10.

58. Loo, S.C., et al., *Synthesis and hydrothermal treatment of nanostructured hydroxyapatite of controllable sizes.* J Mater Sci Mater Med, 2008. **19**(3): p. 1389-97.

59.   Xiao, X.F. and R.F. Liu, *Effect of suspension stability on electrophoretic deposition of hydroxyapatite coatings.* Materials Letters, 2006. **60**(21-22): p. 2627-2632.

60.   Javidi, M., et al., *Studying surface charge and suspension stability of hydroxyapatite powder in isopropyl alcohol to prepare stable suspension for electrophoretic deposition.* Advances in Applied Ceramics, 2013. **108**(4): p. 241-248.

61.   Saunders, R., et al., *Matrix regulation of skeletal cell apoptosis III: mechanism of ion pair-induced apoptosis.* J Cell Biochem, 2007. **100**(3): p. 703-15.

62.   Gao, Y., et al., *Arginine-chitosan/DNA self-assemble nanoparticles for gene delivery: In vitro characteristics and transfection efficiency.* Int J Pharm, 2008. **359**(1-2): p. 241-6.

63.   Yu, F., X. Tang, and M. Pei, *Surface Modification of Hydroxy Carbonate Apatite Nanoparticles with PDMAEMA via Surface-initiated ATRP.* Chemistry Letters, 2013. **42**(5): p. 486-488.

64.   Xie, X., et al., *The Effect of shape on Cellular Uptake of Gold Nanoparticles in the forms of Stars, Rods, and Triangles.* Sci Rep, 2017. **7**(1): p. 3827.

65.   Lee, W.H., et al., *Modulating protein adsorption onto hydroxyapatite particles using different amino acid treatments.* J R Soc Interface, 2012. **9**(70): p. 918-27.

66.   Zhitomirsky, I., *Cathodic electrodeposition of ceramic and organoceramic materials. Fundamental aspects.* Advances in Colloid and Interface Science, 2002. **97**(1): p. 279-317.

67.   Hu, L., Z. Mao, and C. Gao, *Colloidal particles for cellular uptake and delivery.* Journal of Materials Chemistry, 2009. **19**(20).

APPENDIX

Ability as antiGAPDH siRNA delivery system.

To confirm the effectiveness of HAp nanoparticles as miRNA delivery system, the ability of HAp nanoparticles as a delivery system of antiGAPDH siRNA (one of the most commonly used in quantitative gene expression) were determined by quantitative real-time polymerase chain reaction (RT-PCR) analysis.

Firstly, the complexation of HAp nanoparticles with concentration of 20, 50 and 100 ppm and 25 nM anti-GAPDH siRNA were incubated with hMOBs in 6-well plate for 24 h. Cells were also transfected the anti-GAPDH siRNA with Dharmafect® which is a commercial siRNA/miRNA transfection agent to compare with the complex of siRNA/HAp. After treatment, total RNA was extracted by Trizol lysis reagent and dissolved in 10 μL RNAase free water. 1 μg of RNA sample was reverse transcribed into cDNA by ImProm-II® Reverse transcription system. The RT-PCR was performed using FastStart Essential DNA Green Master kit on PCR detection system (MiniOpticon quantitative PCR, Bio-Rad, Hercules, CA). The PCR conditions was 95 $^\circ$C for 1 minute, followed by 40 amplification cycles consisting of 95 $^\circ$C for 45 seconds, 60 $^\circ$C for 60 seconds, 72 $^\circ$C for 90 seconds, and one extension cycle at 72 $^\circ$C for 10 min. All samples were run in duplicate, and GAPDH mRNA expression results were normalized with 18s ribosomal RNA gene as an internal control. Fold changes of GAPDH mRNA relative expression levels were compared with untreated hMOBs as control.

Ability as antiGAPDH siRNA delivery system of HAp nanoparticles.

The ability as antiGAPDH siRNA delivery system of two HAp nanoparticles was examined in order to test the hypothesis that these materials can deliver the miRNA to hMOBs. It is known that siRNA can also regulate gene expression like miRNA by inhibiting the mRNA activity that lead to down-regulation of targeting messenger RNA (mRNA). The result in Figure A1. revealed that compared with the 100 ppm HAp, the mRNA silencing efficiency was dramatically reduced after treated with HAp/siRNA complexes at every concentration, and the influence of their concentrations on this ability was observed in both HAp carriers. Interestingly, siRNA delivery system of 20 ppm elongated HAp (HAp2) significantly exhibited the greatest mRNA inhibition efficiency, and the level was also significantly better than Dharmafect® carrier.

According to the result, the 20 ppm elongated HAp with 100 nm length was suggested as a good efficient carrier for miRNA delivery system.
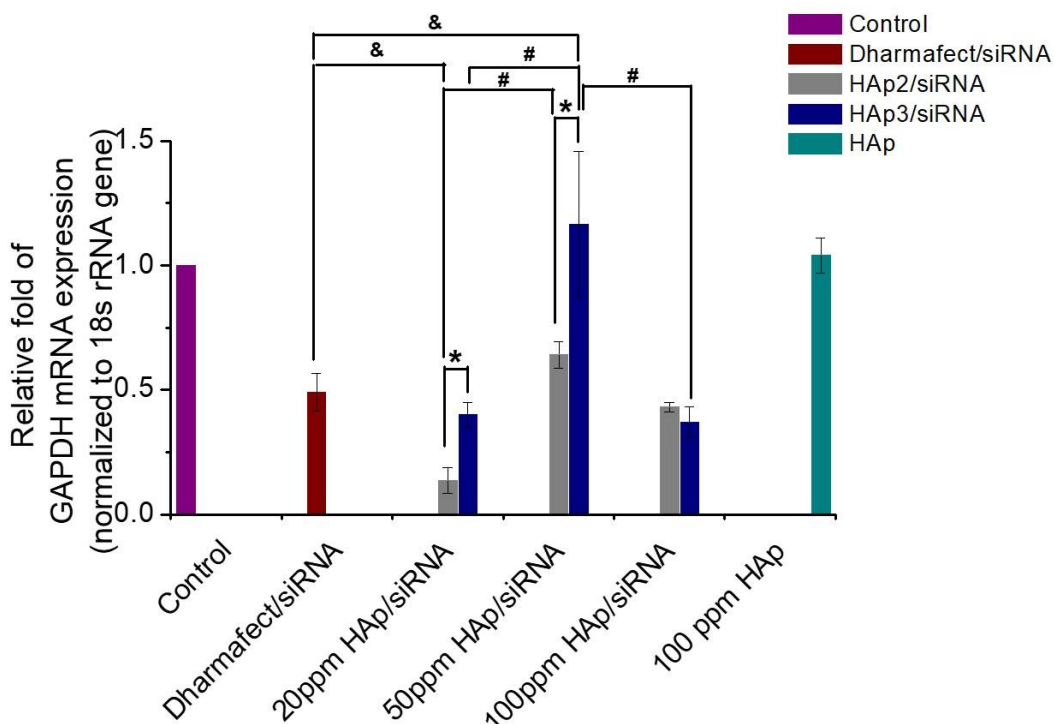

Figure A1. Relative GAPDH mRNA expression level for hMOBs after treated with 20, 50, 100 ppm of HAp nanoparticles as antiGAPDH siRNA vehicle compared to Dharmafect vehicle, results were normalized to the expression of 18s rRNA gene. *, significant difference versus three HAp groups (p < 0.05), #p < 0.05 versus different HAp concentrations and &p < 0.05 versus difference siRNA carrier.

Ability as antiGAPDH siRNA delivery system of modified HAp nanoparticles.

To evaluate whether modified HAp nanoparticles can deliver miRNA to hMOBs, the ability as antiGAPDH siRNA delivery system was investigated as demonstrated in Figure A2. As expected, two positive surfactants grafted particles had an ability to reduce the GAPDH mRNA expression compared to bare HAp/siRNA system. Similar to the above result, the modified HAp concentrations also affected on mRNA inhibition efficiency. The mRNA was notably downregulated when the HAp-APTES/siRNA concentrations were increased, whereas no significant change was observed in HAp-

PDMAEMA/siRNA system. It was found that the 100 ppm HAp-APTES/siRNA complex had the best ability to inhibit the target mRNA in comparison to other siRNA carriers. Consequently, the modified HAp with APTES can be determined as the most suitable miRNA vehicle for high-performance miRNA delivery system.
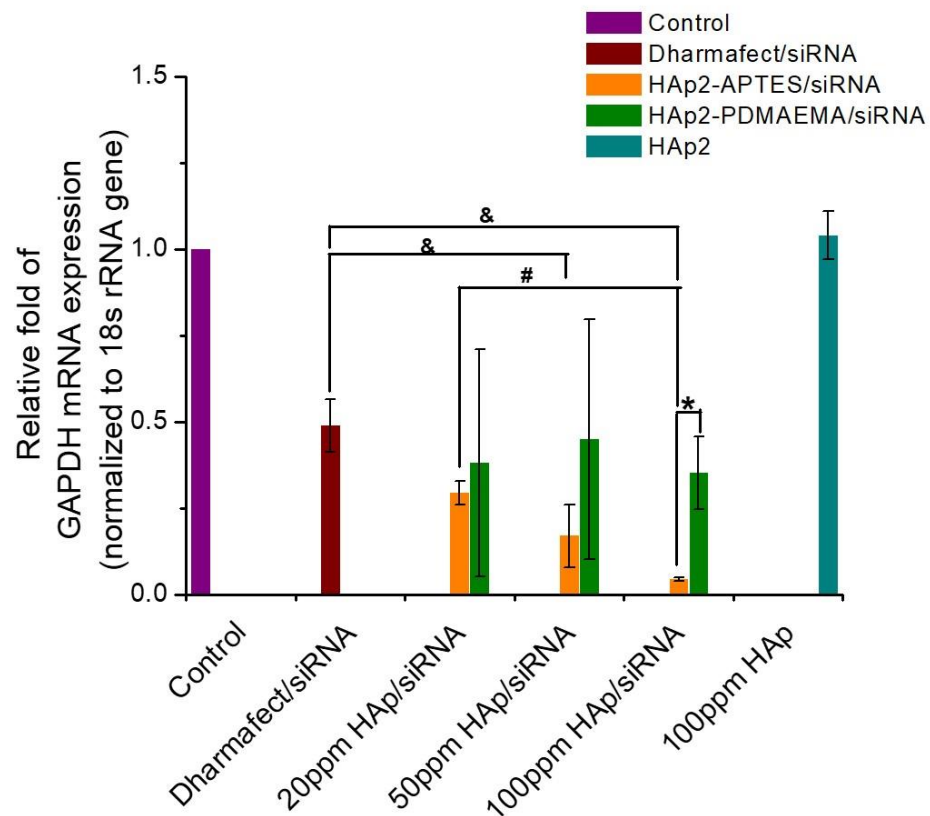

Figure A2. Relative GAPDH mRNA expression level for hMOBs after treated with 20, 50, 100 ppm of unmodified and modified HAp2 nanoparticles as antiGAPDH siRNA vehicle compared to Dharmafect vehicle, results were normalized to the expression of 18s rRNA gene. *, significant difference versus three HAp groups ($p < 0.05$), #$p < 0.05$ versus different HAp concentrations and &$p < 0.05$ versus different siRNA carrier.

VITA

NAME   Natthaya Thepphanao

DATE OF BIRTH   05 July 1992

PLACE OF BIRTH   Buriram

INSTITUTIONS ATTENDED   2011-2015, Bachelor Degree in Chemistry, Faculty of Science, Khon Kaen University

HOME ADDRESS   96 Moo 7, Nong Boat Amphoe Nang Rong, Buriram, Thailand 31110

PUBLICATION   Conference Proceeding in the topic of "THE ROLE OF THE SIZE OF HYDROXYAPATITE NANOPARTICLE ON OSTEOBLAST CELL TOXICITY AND THEIR APPLICATION AS MIRNA CARRIER SYSTEM" at The 44st Congress on Science and Technology of Thailand on 29-31 October 2018, Bangkok International Trade & Exhibition Center (BITEC), Bangkok, Thailand

จุฬาลงกรณ์มหาวิทยาลัย
CHULALONGKORN UNIVERSITY